Hybrid Beamforming Designs for Frequency-Selective mmWave MIMO Systems with Per-RF chain or Per-antenna Power Constraints

Roberto López-Valcarce, *Senior Member, IEEE*, Nuria González-Prelcic, *Senior Member, IEEE*

Abstract—Configuring precoders and combiners is a major challenge to deploy practical multiple-input multiple-output (MIMO) millimeter wave (mmWave) communication systems with large antenna arrays. Most prior work addresses the problem focusing on a total transmit power constraint. In practical transmitters, however, power amplifiers must operate within their linear range, so that a power constraint applies to each one of the input signals to these devices. Therefore, precoder and combiner designs should incorporate per-antenna or per-radio frequency (RF) chain transmit power constraints. We focus on such problem for frequency-selective channels with multicarrier modulation, and assuming hybrid analog/digital architectures based on fully connected analog blocks implemented with finite-resolution phase shifters. We first derive an all-digital solution which aims to maximize spectral efficiency. Then, we develop hybrid precoders and combiners by approximately matching the corresponding all-digital matrices while still enforcing the power constraints. Numerical results show that the proposed all-digital design performs close to the upper bound given by the standard waterfilling-based solution with a total power constraint. Additionally, the hybrid designs exhibit a moderate loss even when low-resolution phase shifters are considered.

Index Terms—Frequency-selective channel, hybrid analog/digital precoding, millimeter wave communications, per-antenna power constraints.

I. INTRODUCTION

Configuring antenna arrays in Multiple-Input Multiple Output (MIMO) mmWave frequency-selective scenarios is a challenging task. The main issues to be addressed are (i) to obtain channel state information (CSI) of sufficient quality, either in terms of spatial covariance or channel estimates; and (ii) to jointly design hybrid architectures, by splitting their operation between the analog and digital domains to reduce the number of radio frequency (RF) chains [1]. The fact that part of the transmit/receive processing must be performed in the analog domain implies that analog hardware limitations must be taken into account, making the precoder and combiner design problem with hybrid architectures significantly harder than its all-digital counterpart. In addition, the analog precoder

R. López-Valcarce is with the atlanTTic Research Center, Universidade de Vigo, 36310 Vigo, Spain. (e-mail: valcarce@gts.uvigo.es).

N. González-Prelcic is with the Department of Electrical and Computer Engineering, North Carolina State University, Raleigh, NC 27695 USA (e-mail: ngprelcic@ncsu.edu).

must accommodate different data streams for the different subcarriers using a small number of RF chains, which results in a small number of degrees of freedom and makes the design problem even harder.

The idea of a hybrid analog-digital solution for the precoders and combiners under a total power constraint was first proposed in [2], and then developed in [3] for sparse narrowband MIMO channels at mmWave frequencies. Perfect factorization of the precoders is obtained in [2], but it requires a large number of RF chains, so that the solution is not feasible at mmWave frequencies. A common approach for mmWave hybrid system design is to approximate the all-digital solution as the product of factors corresponding to the analog and digital stages. Many approaches to this task have been proposed in the literature for the single-user, narrowband case [4]–[6]; however, the mmWave channel is frequency-selective, and multicarrier techniques such as orthogonal frequency division multiplexing (OFDM) become appealing because of their ability to simplify equalization at the receiver and their good pairing with MIMO. With OFDM it is possible to apply individual baseband precoders/combiners in the digital domain on a per-subcarrier basis; however, the analog RF precoder/combiner must necessarily be common for all subcarriers, i.e., it is frequency flat.

A. Prior work

The design of hybrid precoders and combiners for frequency-selective mmWave systems has been recently considered in several works [7]–[15]. The authors of [7] focus on the design of precoder codebooks for limited feedback systems. In [8] the RF precoder/combiner is computed by maximizing the received power, under the assumption that the channel autocorrelation matrices at the different subcarriers can all be approximated by a common autocorrelation matrix constructed from angular information alone, neglecting the time delays of the mmWave channel response. A common autocorrelation matrix obtained by averaging over all subcarriers is analogously used in [9] and [10] to maximize the mutual information with respect to the RF precoder. In [11] and [12] the hybrid precoder is obtained by minimizing the Euclidean distance to an all-digital counterpart computed in turn to minimize the mean squared error (MSE) between transmitted and received signals; this approach is also adopted in [13], [14] for fully-connected phase-shifter based and in [15] for fixed-phase shifters and switches based architectures.

The common limitation of these and similar works is that they assume either per-subcarrier power constraints or a total power constraint. The former are overly restrictive in practice and therefore suffer a performance loss, whereas the latter does not take into account the practical limitations imposed by individual power amplifiers, which may be placed either at each antenna [16]–[18] or at each RF chain [19], [20]. Note that in passive arrays, a high-power RF amplifier is placed at each RF chain, and the array is fed through a low-loss combining network; in contrast, active arrays incorporate a power amplifier at each antenna element [21].

The problem of precoder/combiner design under per-antenna power constraints has been considered in [17], [18], [22], [23] for all-digital structures, and in [19], [24]–[26] for the hybrid architecture. In particular, [24], [25] proposed designs assuming frequency-flat channels, and for fully- and partially-connected architectures, respectively. The design from [19] contemplates both possibilities for the downlink of a multiuser setting, but again assuming frequency-flat channels and without any combiner at the user side, which simplifies the design. To the best of our knowledge, the only hybrid designs for frequency-selective channels under per-antenna or per-RF chain power constraints is our preliminary work in [26] for the fully-connected architecture with per-antenna constraints, and the design from [20] for the partially-connected structure with per-RF chain constraints.

B. Contribution

We propose a novel design for hybrid precoders and combiners in a point-to-point mmWave system with frequency-selective MIMO channels. The RF analog processing is implemented using a fully-connected phase-shifter-based architecture, where the signal at each RF chain is fed to every antenna. Previous hybrid transceiver designs consider the maximization of the mutual information, thus decoupling the designs of the precoder and combiner, and with total or per-subcarrier power constraints; in contrast, we address the problem of directly maximizing the spectral efficiency by jointly designing the precoder and combiner, and under either per-RF chain or per-antenna power constraints. The contributions of this paper are summarized as follows:

- We formulate the problem of finding all-digital precoders and combiners maximizing the spectral efficiency of a MIMO-OFDM system with per-antenna power constraints, in contrast with previous approaches which consider either total or per-subcarrier power constraints. In addition, we consider the maximization of the spectral efficiency as defined in (3) in [3](which depends on both the precoder and combiner), rather than mutual information with an optimal fully digital receiver and no combiner (as defined in (8) in [3]). Thus, in our approach, the precoder and combiner designs are tackled jointly, not separately, in contrast with many methods in the literature which first design the precoder.
- Owing to the non-convex nature of the problem, we propose a tractable approximation. It is seen that adopting a uniform power allocation strategy across streams and

subcarriers does not entail a significant loss with respect to optimum power allocation, while it provides substantial computational savings. The all-digital design provides both a performance upper bound as well as a reference to be matched with hybrid architectures.
- A design criterion is proposed for hybrid combiners with a fully-connected analog network by minimizing the sum over all subcarriers of squared chordal distances between the subspaces defined by the all-digital and hybrid combiners. The approach based on Euclidean (rather than chordal) distances is shown to yield an equivalent design.
- The design of the hybrid precoders is approached using a similar metric, which cannot be interpreted in terms of chordal distances between subspaces anymore, due to the role of the power constraints. Note that it was observed in [7] that minimizing the chordal distance between subspaces is approximately equivalent to maximizing the mutual information, as long as the precoders are constrained to be semi-unitary, which is not the case in our setting.
- The per-antenna or per-RF chain power constraints are efficiently handled by decoupling the role of the different factors in the SVD of the baseband precoders. In particular, their singular values are obtained by maximizing the spectral efficiency in what turns out to be a convex problem.
- We evaluate and compare the performance of the all-digital and hybrid solutions using realistic small-scale parameters directly taken from the 3GPP channel model described in [27]. The hybrid designs show graceful degradation with decreasing phase-shifter resolution.

Our preliminary work in [26] did not include the derivations and expressions of the all-digital precoders and combiners, the uniform power allocation strategy proposed herein, or all the necessary mathematical steps to find their hybrid factorizations. Moreover, the connection between Euclidean and chordal distances in the hybrid designs was not exposed, per-RF chain power constraints were not considered, and presented numerical validation was limited.

Perfect channel estimates are assumed throughout the paper, although it is true that channel estimation errors will unavoidably degrade performance in practice. A number of methods have been recently proposed to efficiently estimate the parameters of the wideband mmWave channel by exploiting its low rank and sparse scattering nature [28]–[31]. Thus, the availability of accurate CSI in this context is certainly not trivial, but not unreasonable.

C. Notation

Bold lowercase $\mathbf{v}$ denotes a column vector, whereas bold uppercase $\mathbf{A}$ is used to denote matrices. $\mathbf{A}^T$ and $\mathbf{A}^*$ stand for the transpose and conjugate transpose of $\mathbf{A}$, respectively. The (i, j)-th entry of matrix $\mathbf{A}$ is denoted as $[\mathbf{A}]_{i,j}$, and the i-th entry of vector $\mathbf{v}$ is denoted as $[\mathbf{v}]_i$. The $n \times n$ identity matrix is denoted as $\mathbf{I}_n$, with $\mathbf{e}_j$ being its j-th column. The Frobenius norm and determinant of $\mathbf{A}$ are respectively denoted as $\|\mathbf{A}\|_F$ and $|\mathbf{A}|$. For $\mathbf{A} \in \mathbb{C}^{n \times n}$ Hermitian, its ordered eigenvalues

are denoted as $\lambda_1(\mathbf{A}) \geq \lambda_2(\mathbf{A}) \geq \cdots \geq \lambda_n(\mathbf{A})$. We use δ_k for the Kronecker delta, $\mathbb{E}$ for expectation, and $\mathcal{CN}(\mu, \mathbf{C})$ for the circularly symmetric complex Gaussian distribution with mean μ and covariance $\mathbf{C}$. Discrete-time and frequency-domain signals are respectively denoted as $\mathbf{x}[n]$ and $\mathbf{x}[k]$.

II. System model

We consider a single-user MIMO-OFDM based hybrid mmWave link employing K subcarriers to send B blocks of symbols $\mathbf{s}_i[k] \in \mathbb{C}^{N_s}$, $k = 0, 1, \ldots, K - 1$, $i = 1, \ldots, B$; thus, i and k denote the block and subcarrier indices, respectively, whereas the number of streams is N_s. Symbols are assumed zero-mean and uncorrelated across blocks and subcarriers, so that $\mathbb{E}\{\mathbf{s}_i[k]\mathbf{s}_j^*[k']\} = \frac{P}{KN_s}\mathbf{I}_{N_s}\delta_{i-j}\delta_{k-k'}$ with P the average total transmit power. The transmitter has N_t antennas, whereas the receiver is equipped with N_r antennas. The system is based on a hybrid architecture as shown in Fig. 1, with L_t and L_r RF chains at the transmitter and receiver sides, respectively. At the transmitter, a frequency-selective hybrid precoder $\mathbf{F}[k] \in \mathbb{C}^{N_t \times N_s}$ is used, with $\mathbf{F}[k] = \mathbf{F}_{RF}\mathbf{F}_{BB}[k]$, $k = 0, \ldots, K - 1$. Here $\mathbf{F}_{RF} \in \mathbb{C}^{N_t \times L_t}$ is the analog precoder, which is frequency-flat, and $\mathbf{F}_{BB}[k] \in \mathbb{C}^{L_t \times N_s}$ are the digital precoders, which may vary across subcarriers.

Symbol blocks are transformed into the time domain using L_t parallel K-point IFFTs. The time-domain samples of the transmitted baseband-equivalent signal can be expressed as

$$\mathbf{x}[n] = \frac{1}{\sqrt{K}}\mathbf{F}_{RF}\sum_{i=1}^{B}\sum_{k=0}^{K-1}\mathbf{F}_{BB}[k]\mathbf{s}_i[k]$$
$$\times e^{j\frac{2\pi}{K}k(n-Z_{CP}-i(K+Z_{CP}))}w[n - i(K + Z_{CP})], \quad (1)$$

where Z_{CP} is the cyclic prefix length, and $w[n]$ is the length-$(K + Z_{CP})$ rectangular pulse defined as $w[n] = 1$ for $n = 0, \ldots, K + Z_{CP} - 1$, and 0 otherwise.

The MIMO channel between transmitter and receiver is assumed to be frequency-selective, with impulse response length not exceeding the cyclic prefix length. Let ρ_L be the path loss, C and R_c the number of clusters and rays in the c-th cluster, respectively, T_s the sampling interval, and $p(t)$ the impulse response of a filter including the effects of pulse-shaping and other analog filtering. Also let $\alpha_{c,r} \in \mathbb{C}$, $\tau_{c,r} \in \mathbb{R}$, $\phi_{c,r} \in [0, 2\pi)$ and $\theta_{c,r} \in [0, 2\pi)$ be respectively the complex gain, delay, and angles-of-arrival and departure (AoA/AoD) of the r-th path in the c-th cluster, and $\mathbf{a}_R(\phi) \in \mathbb{C}^{N_r}$, $\mathbf{a}_T(\theta) \in \mathbb{C}^{N_t}$ be the steering vectors of the receive and transmit arrays. Then, the d-th delay tap of the channel is given by an $N_r \times N_t$ matrix denoted as $\mathbf{H}_d$, which, assuming a geometric channel model [32], can be written as

$$\mathbf{H}_d = \sqrt{\frac{N_t N_r}{\rho_L R}}\sum_{c=1}^{C}\sum_{r=1}^{R_c}\alpha_{c,r}p(dT_s - \tau_{c,r})\mathbf{a}_R(\phi_{c,r})\mathbf{a}_T^*(\theta_{c,r}), \quad (2)$$

with $R \triangleq \sum_{c=1}^{C} R_c$ the total number of paths. Now, $\mathbf{H}_d$ in (2) can be written more compactly as

$$\mathbf{H}_d = \mathbf{A}_R \mathbf{G}_d \mathbf{A}_T^*, \quad (3)$$

where $\mathbf{G}_d \in \mathbb{C}^{R \times R}$ is diagonal, and the columns of $\mathbf{A}_R \in \mathbb{C}^{N_r \times R}$ and $\mathbf{A}_T \in \mathbb{C}^{N_t \times R}$ comprise the receive and transmit

array steering vectors $\mathbf{a}_R(\phi_{c,r})$ and $\mathbf{a}_T(\theta_{c,r})$, respectively. The frequency-domain $N_r \times N_t$ MIMO channel matrix at subcarrier k is then given by

$$\mathbf{H}[k] = \sum_{d=0}^{N_c-1}\mathbf{H}_d e^{-j\frac{2\pi k}{K}d} = \mathbf{A}_R \mathbf{G}[k]\mathbf{A}_T^*, \quad (4)$$

where N_c is the number of channel taps in the time domain, and $\mathbf{G}[k] \triangleq \sum_{d=0}^{N_c-1} \mathbf{G}_d e^{-j\frac{2\pi k}{K}d}$.

In the wideband regime, the array response vectors become frequency-dependent, an effect known as *beam-squint* [33], [34]. In this case, the signal wavelength is subcarrier dependent: $\lambda_k = \frac{c}{\frac{kB}{K} + f_c - \frac{B}{2}}$, where c, B and f_c denote the propagation speed, the bandwidth, and the carrier frequency, respectively. For example, in the case of a uniform linear array (ULA) with d-spaced elements at the transmit side, the steering vector at the k-th subcarrier becomes

$$\left[\mathbf{a}_{T,k}(\theta)\right]_m = \frac{1}{\sqrt{N_t}}e^{-j\frac{2\pi d}{\lambda_k}m\sin\theta}, \quad m = 0, 1, \ldots, N_t - 1. \quad (5)$$

An analogous expression applies to the receive array response vectors $\mathbf{a}_{R,k}(\phi)$. The channel matrices in (4) must be modified to account for this effect, so that now one has

$$\mathbf{H}[k] = \mathbf{A}_R[k]\mathbf{G}[k]\mathbf{A}_T^*[k], \quad (6)$$

where $\mathbf{A}_R[k]$ and $\mathbf{A}_T[k]$ respectively comprise the receive and transmit array steering vectors $\mathbf{a}_{R,k}(\phi_{c,r})$ and $\mathbf{a}_{T,k}(\theta_{c,r})$.

The receiver applies a hybrid combiner $\mathbf{W}[k] = \mathbf{W}_{RF}\mathbf{W}_{BB}[k] \in \mathbb{C}^{N_r \times N_s}$, with $\mathbf{W}_{RF} \in \mathbb{C}^{N_r \times L_r}$ the analog combiner common to all subcarriers, and $\mathbf{W}_{BB}[k] \in \mathbb{C}^{L_r \times N_s}$ the digital factor. Then, assuming the channel impulse response is shorter than the cyclic prefix as well as perfect synchronization, after cyclic prefix removal and FFT processing, the received signal at subcarrier k of the i-th OFDM symbol can be written as

$$\mathbf{y}_i[k] = \mathbf{W}_{BB}^*[k]\mathbf{W}_{RF}^*\mathbf{H}[k]\mathbf{F}_{RF}\mathbf{F}_{BB}[k]\mathbf{s}_i[k] + \mathbf{W}_{BB}^*[k]\mathbf{W}_{RF}^*\mathbf{n}_i[k],$$
$$(7)$$

where $\mathbf{n}_i[k] \sim \mathcal{CN}(\mathbf{0}, \sigma^2\mathbf{I})$ is the additive noise. Channel matrices are assumed normalized according to

$$\frac{1}{K}\sum_{k=0}^{K-1}\|\mathbf{H}[k]\|_F^2 = N_t N_r. \quad (8)$$

III. Problem formulation

We assume perfect channel state information (CSI) at the transmitter and receiver, and focus on the problem of designing hybrid precoders and combiners maximizing the spectral efficiency (or, equivalently, the achievable rate), subject to per-antenna or per-RF chain power constraints. Under Gaussian signaling, the spectral efficiency corresponding to (7) can be expressed as

$$\mathcal{R} = \frac{1}{K}\sum_{k=0}^{K-1}\log_2\left|\mathbf{I}_{N_s} + \frac{\text{SNR}}{N_s}(\mathbf{W}^*[k]\mathbf{W}[k])^{-1}\right.$$
$$\left. \times \mathbf{W}^*[k]\mathbf{H}[k]\mathbf{F}[k]\mathbf{F}^*[k]\mathbf{H}^*[k]\mathbf{W}[k]\right|, \quad (9)$$

where $\text{SNR} \triangleq \frac{P}{K\sigma^2}$. To find the average power at each transmit antenna, let us define $\mathbf{x}_i[k] = \mathbf{F}[k]\mathbf{s}_i[k]$. Then, the signal
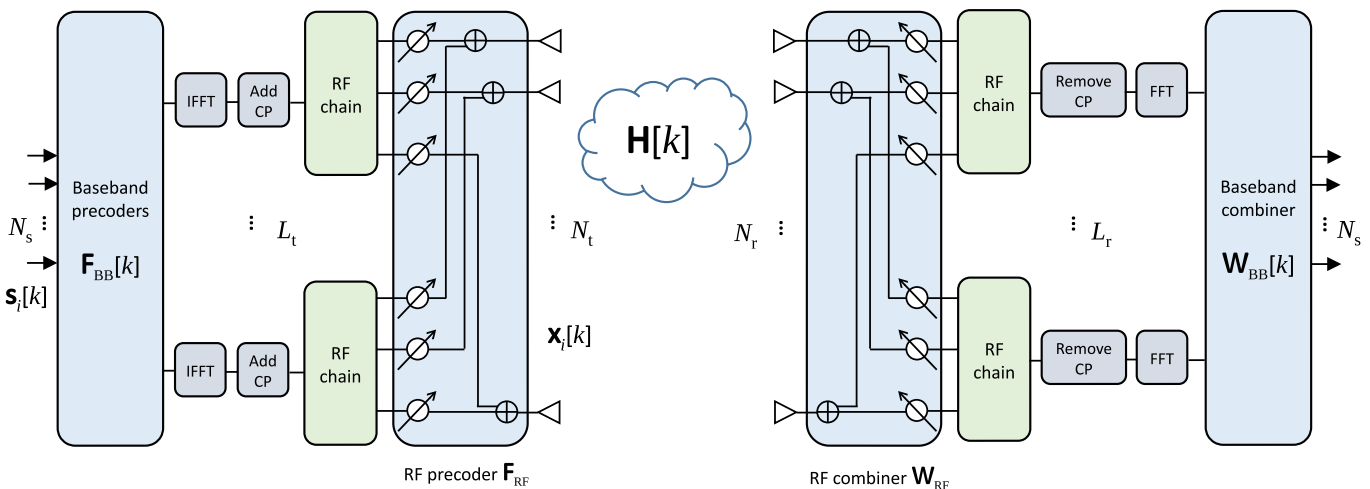
Fig. 1: Structure of a hybrid MIMO-OFDM fully-connected architecture, which includes analog and digital precoders and combiners.

corresponding to the i-th OFDM symbol transmitted through the j-th antenna is the cyclically-extended K-point IDFT of a vector with entries $\mathbf{e}_j^*\mathbf{x}_i[k]$, $k = 0, 1, \ldots, K - 1$. Since the IDFT is a unitary transformation, the average power constraint at the j-th transmit antenna can be written as

$$\sum_{k=0}^{K-1} \mathbb{E}\{|\mathbf{e}_j^*\mathbf{x}_i[k]|^2\} \leq p_j, \qquad \forall j \in \{1, \ldots, N_t\}, \qquad (10)$$

where $p_j > 0$ is the maximum available power at the j-th antenna, with $\sum_{j=1}^{N_t} p_j = P$. Taking into account that $\mathbb{E}\{\mathbf{s}_i[k]\mathbf{s}_i^*[k]\} = \frac{P}{KN_s}\mathbf{I}_{N_s}$, and with $\bar{p}_j \triangleq p_j/P$, (10) can be rewritten as

$$\frac{1}{KN_s}\mathbf{e}_j^* \left(\sum_{k=0}^{K-1} \mathbf{F}[k]\mathbf{F}^*[k]\right)\mathbf{e}_j \leq \bar{p}_j, \quad \forall j \in \{1, \ldots, N_t\}. \quad (11)$$

With hybrid precoders $\mathbf{F}[k] = \mathbf{F}_{RF}\mathbf{F}_{BB}[k]$, let $\widetilde{\mathbf{x}}_i[k] = \mathbf{F}_{BB}[k]\mathbf{s}_i[k]$. If per-RF chain power constraints apply with $q_\ell > 0$ the available power at the ℓ-th RF chain with $\sum_{\ell=1}^{L_t} q_\ell = \frac{P}{N_t}$, then

$$\sum_{k=0}^{K-1} \mathbb{E}\{|\mathbf{e}_\ell^*\widetilde{\mathbf{x}}_i[k]|^2\} \leq q_\ell, \qquad \forall \ell \in \{1, \ldots, L_t\}, \qquad (12)$$

which, letting $\bar{q}_\ell \triangleq q_\ell/P$, translates into

$$\frac{1}{KN_s}\mathbf{e}_\ell^* \left(\sum_{k=0}^{K-1} \mathbf{F}_{BB}[k]\mathbf{F}_{BB}^*[k]\right)\mathbf{e}_\ell \leq \bar{q}_\ell, \qquad \forall \ell \in \{1, \ldots, L_t\}. \tag{13}$$

Besides the power constraints (11) or (13), additional hardware constraints imposed by the analog precoding and combining stages must also be taken into account. We assume that transmitter and receiver employ fully-connected hybrid architectures, as shown in Fig. 1. The analog precoder and combiner are implemented using a fully-connected network of phase shifters, as described in [35], with resolution of b_t and b_r bits, respectively. Let $\mathcal{M}_b^{N \times L}$ denote the set of $N \times L$ matrices with entries having unit magnitude and with phase in the set $\left\{0, \frac{2\pi}{2^b}, \ldots, \frac{2\pi \cdot (2^b - 1)}{2^b}\right\}$, corresponding to b quantization

bits. Then, the analog precoder and combiner must satisfy $\mathbf{F}_{RF} \in \mathcal{M}_{b_t}^{N_t \times L_t}$ and $\mathbf{W}_{RF} \in \mathcal{M}_{b_r}^{N_r \times L_r}$. As a consequence, it turns out in particular that the analog precoder satisfies $\mathbf{F}_{RF}^*\mathbf{F}_{RF} \approx N_t\mathbf{I}_{L_t}$ with high probability [10, Lemma 1].

Note that the total transmit power is given by

$$P_{TX} = \sum_{k=0}^{K-1} \mathbb{E}\{\|\mathbf{x}_i[k]\|^2\} = \frac{P}{KN_s} \text{tr}\left(\sum_{k=0}^{K-1} \mathbf{F}[k]\mathbf{F}^*[k]\right). \quad (14)$$

Under the per-antenna power constraints (10)-(11) with $\sum_{j=1}^{N_t} p_j = P$, $P_{TX} \leq P$ automatically holds. On the other hand, under per-RF chain power constraints (12)-(13) with $\sum_{\ell=1}^{L_t} q_\ell = \frac{P}{N_t}$,

$$
\begin{aligned}
P_{TX} &= \frac{P}{KN_s} \text{tr}\left(\sum_{k=0}^{K-1} \mathbf{F}_{RF}\mathbf{F}_{BB}[k]\mathbf{F}_{BB}^*[k]\mathbf{F}_{RF}^*\right) \\
&\approx \frac{N_t P}{KN_s} \text{tr}\left(\sum_{k=0}^{K-1} \mathbf{F}_{BB}[k]\mathbf{F}_{BB}^*[k]\right) \leq P, \qquad (15)
\end{aligned}
$$

where we have used the cyclic property of the trace, $\text{tr}(\mathbf{AB}) = \text{tr}(\mathbf{BA})$, and the aforementioned property $\mathbf{F}_{RF}^*\mathbf{F}_{RF} \approx N_t\mathbf{I}_{L_t}$. Thus, the normalizations $\sum_{j=1}^{N_t} p_j = P$ and $\sum_{\ell=1}^{L_t} q_\ell = \frac{P}{N_t}$ are appropriate.

Incorporating the hardware-specific constraints into the optimization results in an intractable problem, so we will initially drop them to gain some insight into the design of precoders and combiners under the per-antenna/RF chain power constraints. Thereafter, we will focus on finding the frequency-selective hybrid approximations that are best matched to the all-digital solution.

IV. ALL-DIGITAL DESIGN

Consider an all-digital implementation of the precoder and combiner, corresponding to a system with a dedicated RF chain per antenna. In that case, per-antenna and per-RF chain power constraints become essentially the same, so we focus on the former for concreteness. The problem of jointly

$$\max_{\{\mathbf{W}[k],\mathbf{U}_F[k],\mathbf{\Sigma}_F[k]\}} \frac{1}{K} \sum_{k=0}^{K-1} \log_2 \left| \mathbf{I}_{N_s} + \frac{\text{SNR}}{N_s} \mathbf{W}[k]\mathbf{W}^*[k]\mathbf{H}[k]\mathbf{U}_F[k]\mathbf{\Sigma}_F^2[k]\mathbf{U}_F^*[k]\mathbf{H}^*[k] \right|$$

$$\text{s. to} \quad \begin{cases} \mathbf{W}^*[k]\mathbf{W}[k] = \mathbf{I}_{N_s}, \quad \mathbf{U}_F^*[k]\mathbf{U}_F[k] = \mathbf{I}_{N_s}, \quad \forall k, \\ \frac{1}{KN_s}\mathbf{e}_j^* \left(\sum_{k=0}^{K-1} \mathbf{U}_F[k]\mathbf{\Sigma}_F^2[k]\mathbf{U}_F^*[k] \right) \mathbf{e}_j \le \bar{p}_j, \quad \forall j \in \{1,\dots,N_t\}. \end{cases}$$

(17)

maximizing the spectral efficiency $\mathcal{R}$ under per-antenna power constraints can be stated as

$$\max_{\{\mathbf{F}[k],\mathbf{W}[k]\}} \mathcal{R} \quad \text{s. to} \quad \frac{1}{KN_s}\mathbf{e}_j^* \left(\sum_{k=0}^{K-1} \mathbf{F}[k]\mathbf{F}^*[k] \right) \mathbf{e}_j \le \bar{p}_j,$$
$$\forall j \in \{1,\dots,N_t\}. \quad (16)$$

The closed-form solution to (16) is unknown[1] even for the narrowband case [24]. Following the philosophy in [24], we extend its formulation to the frequency-selective scenario, starting with the result from [24, Lemma 1]; see Appendix A for the proof.

Lemma 1. *The optimal all-digital precoder for problem (16) satisfies all the per-antenna power constraints with equality.*

Next we make the following observations regarding problem (16) based on the expression of $\mathcal{R}$ in (9):

- Using Sylvester's determinant identity, $\mathcal{R}$ is seen to depend on the combiner $\mathbf{W}[k]$ only through the matrix $\mathbf{W}[k](\mathbf{W}^*[k]\mathbf{W}[k])^{-1}\mathbf{W}^*[k]$, which is the orthogonal projector onto the subspace spanned by the columns of $\mathbf{W}[k]$; whereas the power constraints in (16) do not depend on $\mathbf{W}[k]$. Hence, there is no loss of generality in assuming $\mathbf{W}[k]$ semi-unitary, i.e., $\mathbf{W}^*[k]\mathbf{W}[k] = \mathbf{I}_{N_s}$.
- Both $\mathcal{R}$ and the power constraints in (16) depend on the precoder $\mathbf{F}[k]$ only through the matrix $\mathbf{F}[k]\mathbf{F}^*[k]$. Thus, without loss of generality $\mathbf{F}[k]$ can be assumed of the form $\mathbf{U}_F[k]\mathbf{\Sigma}_F[k]$, where $\mathbf{U}_F[k] \in \mathbb{C}^{N_t \times N_s}$ is semi-unitary and $\mathbf{\Sigma}_F[k] \in \mathbb{R}^{N_s \times N_s}$ is diagonal and positive semi-definite, containing the singular values of $\mathbf{F}[k]$ in descending order.

In view of these, (16) can be rewritten as (17) at the top of this page. The main difficulty towards solving (17) is that the semi-unitary part of the precoders, $\mathbf{U}_F[k]$, affects the power constraints. We propose to obtain an approximate solution by the following two-step procedure:

- *Step 1:* First, maximize the objective in (17) with respect to the semi-unitary matrices $\{\mathbf{W}[k],\mathbf{U}_F[k]\}$ neglecting the per-antenna power constraints.
- *Step 2:* Substituting the optimal values from the previous step, maximize the objective with respect to $\{\mathbf{\Sigma}_F[k]\}$ under the per-antenna power constraints.

Note that the solution obtained in this way is feasible for problem (17), although suboptimal in general. Step 1 is solved via the following result, whose proof is given in Appendix B.

[1]The related problem of maximizing the *mutual information* with respect to the precoder was solved in [18] for the narrowband case.

Theorem 1. *For given matrices* $\{\mathbf{H}[k],\mathbf{\Sigma}_F^2[k]\}$, *with each* $\mathbf{\Sigma}_F^2[k]$ *diagonal with non-negative elements in descending order, consider the problem*

$$\max_{\{\mathbf{W}[k],\mathbf{U}_F[k]\}} \frac{1}{K} \sum_{k=0}^{K-1} \log_2 \left| \mathbf{I}_{N_s} + \frac{\text{SNR}}{N_s}\mathbf{W}[k]\mathbf{W}^*[k] \right.$$
$$\left. \times \mathbf{H}[k]\mathbf{U}_F[k]\mathbf{\Sigma}_F^2[k]\mathbf{U}_F^*[k]\mathbf{H}^*[k] \right| \quad (18)$$
$$\text{s. to} \quad \mathbf{W}^*[k]\mathbf{W}[k] = \mathbf{I}_{N_s}, \ \mathbf{U}_F^*[k]\mathbf{U}_F[k] = \mathbf{I}_{N_s}.$$

Let $\widetilde{\mathbf{U}}_H[k] \in \mathbb{C}^{N_r \times N_s}$, $\widetilde{\mathbf{V}}_H[k] \in \mathbb{C}^{N_t \times N_s}$ *respectively comprise the principal* N_s *left and right singular vectors of* $\mathbf{H}[k]$. *The solution to (18) is independent of* $\{\mathbf{\Sigma}_F^2[k]\}$, *and given by*

$$\mathbf{U}_F[k] = \widetilde{\mathbf{V}}_H[k], \quad \mathbf{W}[k] = \widetilde{\mathbf{U}}_H[k], \quad 0 \le k \le K-1. \quad (19)$$

In words, Theorem 1 states that whenever the power allocation strategy does not affect the semi-unitary part of the precoders, the spectral efficiency is maximized by diagonalizing the channels. The application to the case of a total power constraint is well known, in which the precoders' singular values are obtained via waterfilling.

Let $\widetilde{\mathbf{\Sigma}}_H[k]$ be a diagonal matrix with the N_s largest singular values of $\mathbf{H}[k]$, in descending order. Then, with the values for $\{\mathbf{U}_F[k],\mathbf{W}[k]\}$ from (19), Step 2 amounts to solving

$$\max_{\{\mathbf{\Sigma}_F[k]\}} \frac{1}{K} \sum_{k=0}^{K-1} \log_2 \left| \mathbf{I}_{N_s} + \frac{\text{SNR}}{N_s}\mathbf{\Sigma}_F^2[k]\widetilde{\mathbf{\Sigma}}_H^2[k] \right|$$
$$\text{s. to} \quad \frac{1}{KN_s}\mathbf{e}_j^* \left(\sum_{k=0}^{K-1} \widetilde{\mathbf{V}}_H[k]\mathbf{\Sigma}_F^2[k]\widetilde{\mathbf{V}}_H^*[k] \right) \mathbf{e}_j \le \bar{p}_j, \ \forall j. \quad (20)$$

Denoting the (j,i)-th element of $\widetilde{\mathbf{V}}_H[k]$ by $v_{ji}[k]$, $1 \le j \le N_t$, $1 \le i \le N_s$, and the i-th diagonal entries of $\widetilde{\mathbf{\Sigma}}_H[k]$, $\mathbf{\Sigma}_F[k]$ by $\sigma_{H,i}[k]$, $\rho_i[k]$ respectively, problem (20) becomes

$$\max_{\{\rho_i^2[k]\}} \frac{1}{K} \sum_{k=0}^{K-1} \sum_{i=1}^{N_s} \log_2 \left(1 + \frac{\text{SNR}}{N_s}\sigma_{H,i}^2[k]\rho_i^2[k] \right)$$
$$\text{s. to} \quad \frac{1}{KN_s} \sum_{k=0}^{K-1} \sum_{i=1}^{N_s} |v_{ji}[k]|^2 \rho_i^2[k] \le \bar{p}_j, \ \forall j. \quad (21)$$

Problem (21) is convex in the power allocation coefficients $\{\rho_i[k]\}$, so it can be solved using any convex optimization tool. The result is a space-frequency power allocation algorithm, in which the effective per-subcarrier SNR determines how the per-antenna power budget is split into the different subchannels. In general, the solution to (21) need not satisfy all the power constraints with equality, and thus, in view of Lemma 1, the proposed all-digital design need not be optimal in terms of the original problem (17).

Algorithm 1 All-digital design under per-antenna power constraints

---

Input: Channel coefficients $\{\mathbf{H}[k]\}_{k=0}^{K-1}$, available powers $\{\bar{p}_j\}_{j=1}^{N_t}$

for $k = 0, \ldots, K-1$ **do**

　　Set $\widetilde{\mathbf{V}}_H[k] \leftarrow N_s$ principal right singular vectors of $\mathbf{H}[k]$

　　Set $\widetilde{\boldsymbol{\Sigma}}_H[k] \leftarrow$ diagonal with the N_s largest singular values of $\mathbf{H}[k]$

　　Set $\mathbf{W}[k] \leftarrow N_s$ principal left singular vectors of $\mathbf{H}[k]$

end for

Non-uniform power allocation: Solve for $\{\boldsymbol{\Sigma}_F[k]\}_{k=0}^{K-1}$ in (20) or, equivalently, (21)

Uniform power allocation: Compute ρ^2 via (23)

for $k = 0, \ldots, K-1$ **do**

　　Non-uniform power alloc.: Set $\mathbf{F}[k] = \widetilde{\mathbf{V}}_H[k]\boldsymbol{\Sigma}_F[k]$

　　Uniform power alloc.: Set $\mathbf{F}[k] = \rho\widetilde{\mathbf{V}}_H[k]$

end for

Output: all-digital precoders $\{\mathbf{F}[k]\}_{k=0}^{K-1}$, all-digital combiners $\{\mathbf{W}[k]\}_{k=0}^{K-1}$

Despite the convexity of (21), the number of optimization variables KN_s can be large, which may hamper the application of this design in practice. Seeking a more favorable tradeoff between performance and complexity, we propose an alternative approach with uniform power allocation across data streams and subcarriers, by imposing $\rho_i[k] = \rho$ for all i and k in (21). In this way, a single variable ρ has to be optimized by solving

$$
\max_{\rho^2 \geq 0} \frac{1}{K} \sum_{k=0}^{K-1} \sum_{i=1}^{N_s} \log_2 \left(1 + \frac{\text{SNR}}{N_s} \sigma_{H,i}^2[k]\rho^2 \right)
$$
$$
\text{s. to } \frac{1}{KN_s} \sum_{k=0}^{K-1} \sum_{i=1}^{N_s} |v_{ji}[k]|^2 \rho^2 \leq \bar{p}_j, \ \forall j. \tag{22}
$$

Since each of the log terms in the objective of (22) is monotonically increasing in ρ^2, the optimum is achieved by the largest feasible value of ρ^2, given in closed form by

$$
\rho^2 = KN_s \min_{1 \leq j \leq N_t} \frac{\bar{p}_j}{\mathbf{e}_j^* \left(\sum_{k=0}^{K-1} \widetilde{\mathbf{V}}_H[k]\widetilde{\mathbf{V}}_H^*[k] \right) \mathbf{e}_j}. \tag{23}
$$

The all-digital design is summarized in Algorithm 1. With the uniform power allocation approach (23), its computational load is dominated by the K SVDs of the channel matrices, and thus it is $O(K \min(N_t^2 N_r, N_r^2 N_t))$. With non-uniform power allocation, the cost of solving (21) has to be additionally considered. This cost will depend on the chosen convex solver and is difficult to quantify, but as the number of subcarriers K increases it will tend to become dominant, since the number of optimization variables is KN_s. Results given in Sec. VII will show that the performance loss incurred by the uniform power allocation approach (23) is rather small.

V. DESIGN OF FREQUENCY-SELECTIVE HYBRID COMBINERS

We follow two different approaches for the design of the frequency-selective hybrid combiners $\mathbf{W}_{\text{RF}}\mathbf{W}_{\text{BB}}[k]$, which will be shown to be equivalent in terms of spectral efficiency. Consider the all-digital solution $\mathbf{W}[k] = \widetilde{\mathbf{U}}_H[k]$ from Theorem 1, which is semi-unitary for all k, and note that the spectral efficiency (9) depends on this all-digital combiner only through the orthogonal projection matrices $\mathbf{W}[k](\mathbf{W}^*[k]\mathbf{W}[k])^{-1}\mathbf{W}^*[k] = \mathbf{W}[k]\mathbf{W}^*[k]$. This motivates a first approach in which these projection matrices are approximated, i.e., $\mathbf{W}_{\text{RF}}\mathbf{W}_{\text{BB}}[k] (\mathbf{W}_{\text{RF}}\mathbf{W}_{\text{BB}}[k])^* \approx \mathbf{W}[k]\mathbf{W}^*[k]$. The second approach directly attempts to match the combiners, i.e., $\mathbf{W}_{\text{RF}}\mathbf{W}_{\text{BB}}[k] \approx \mathbf{W}[k]$ for all k. In both cases we use the Euclidean distance as the metric in the approximation.

Since the factor $\mathbf{W}_{\text{RF}} \in \mathbb{C}^{N_r \times L_r}$ of the hybrid combiner is common to all subcarriers, we are basically looking for an L_r-dimensional subspace (the one spanned by the columns of $\mathbf{W}_{\text{RF}}$) which approximately contains all of the N_s-dimensional subspaces spanned by $\mathbf{W}[k]$, $k = 0, \ldots, K-1$. In addition, the subspace sought should have a basis with the special structure imposed by the hardware constraints; having a larger number of RF chains L_r should improve the approximation.

A. Approximation of projection matrices

In this approach, the hybrid combiner is the solution to

$$
\min_{\mathbf{W}_{\text{RF}}, \{\mathbf{W}_{\text{BB}}[k]\}} \frac{1}{2} \sum_{k=0}^{K-1} \big\| \mathbf{W}[k]\mathbf{W}^*[k]
$$
$$
- \mathbf{W}_{\text{RF}}\mathbf{W}_{\text{BB}}[k] (\mathbf{W}_{\text{RF}}\mathbf{W}_{\text{BB}}[k])^* \big\|_F^2 \tag{24}
$$
$$
\text{s. to } \begin{cases} \mathbf{W}_{\text{RF}} \in \mathcal{M}_{b_r}^{N_r \times L_r}, \\ (\mathbf{W}_{\text{RF}}\mathbf{W}_{\text{BB}}[k])^* (\mathbf{W}_{\text{RF}}\mathbf{W}_{\text{BB}}[k]) = \mathbf{I}_{N_s} \ \forall k. \end{cases}
$$

The cost function in (24) is the sum of squared extrinsic distances between the subspaces spanned by the columns of $\mathbf{W}[k]$ and $\mathbf{W}_{\text{RF}}\mathbf{W}_{\text{BB}}[k]$; since these subspaces have the same dimension N_s, the extrinsic distance is equivalent to the chordal distance [36]. Developing (24), and using the fact that $\mathbf{W}[k]$ and $\mathbf{W}_{\text{RF}}\mathbf{W}_{\text{BB}}[k]$ are semi-unitary, it is found that

$$
\frac{1}{2} \sum_{k=0}^{K-1} \big\| \mathbf{W}[k]\mathbf{W}^*[k] - \mathbf{W}_{\text{RF}}\mathbf{W}_{\text{BB}}[k] (\mathbf{W}_{\text{RF}}\mathbf{W}_{\text{BB}}[k])^* \big\|_F^2
$$
$$
= KN_s - \sum_{k=0}^{K-1} \big\| \mathbf{W}^*[k]\mathbf{W}_{\text{RF}}\mathbf{W}_{\text{BB}}[k] \big\|_F^2. \tag{25}
$$

The main difficulty when attempting to solve (24) lies in the constraint $\mathbf{W}_{\text{RF}} \in \mathcal{M}_{b_r}^{N_r \times L_r}$. Thus, we drop it for the moment, and will eventually enforce it by projecting the obtained solution onto $\mathcal{M}_{b_r}^{N_r \times L_r}$, as usual. In view of (25), the corresponding problem reads as

$$
\max_{\mathbf{W}_{\text{RF}}, \{\mathbf{W}_{\text{BB}}[k]\}} \sum_{k=0}^{K-1} \big\| \mathbf{W}^*[k]\mathbf{W}_{\text{RF}}\mathbf{W}_{\text{BB}}[k] \big\|_F^2 \tag{26}
$$
$$
\text{s. to } (\mathbf{W}_{\text{RF}}\mathbf{W}_{\text{BB}}[k])^* (\mathbf{W}_{\text{RF}}\mathbf{W}_{\text{BB}}[k]) = \mathbf{I}_{N_s} \ \forall k.
$$

Consider now the SVD $\mathbf{W}_{RF} = \mathbf{U}_W \boldsymbol{\Sigma}_W \mathbf{V}_W^*$, with $\mathbf{U}_W \in \mathbb{C}^{N_r \times L_r}$ and $\boldsymbol{\Sigma}_W$, $\mathbf{V}_W \in \mathbb{C}^{L_r \times L_r}$, and let $\widetilde{\mathbf{W}}_{BB}[k] \triangleq \boldsymbol{\Sigma}_W \mathbf{V}_W^* \mathbf{W}_{BB}[k]$. Since $\mathbf{U}_W^* \mathbf{U}_W = \mathbf{I}_{L_r}$, we can rewrite (26) as

$$\max_{\mathbf{U}_W, \{\widetilde{\mathbf{W}}_{BB}[k]\}} \sum_{k=0}^{K-1} \left\| \mathbf{W}^*[k] \mathbf{U}_W \widetilde{\mathbf{W}}_{BB}[k] \right\|_F^2 \tag{27}$$
$$\text{s. to} \begin{cases} \mathbf{U}_W^* \mathbf{U}_W = \mathbf{I}_{L_r}, \\ (\widetilde{\mathbf{W}}_{BB}[k])^* \widetilde{\mathbf{W}}_{BB}[k] = \mathbf{I}_{N_s} \; \forall k. \end{cases}$$

Using Von Neumann's trace inequality [37, Th. 7.4.1.1], for any semi-unitary matrices $\{\widetilde{\mathbf{W}}_{BB}[k]\}$ the objective in (27) can be upper bounded as

$$\sum_{k=0}^{K-1} \left\| \mathbf{W}^*[k] \mathbf{U}_W \widetilde{\mathbf{W}}_{BB}[k] \right\|_F^2$$
$$= \sum_{k=0}^{K-1} \text{tr} \left\{ \widetilde{\mathbf{W}}_{BB}^*[k] \mathbf{U}_W^* \mathbf{W}[k] \mathbf{W}^*[k] \mathbf{U}_W \widetilde{\mathbf{W}}_{BB}[k] \right\}$$
$$\leq \sum_{k=0}^{K-1} \sum_{i=1}^{N_s} \lambda_i \left(\mathbf{U}_W^* \mathbf{W}[k] \mathbf{W}^*[k] \mathbf{U}_W \right). \tag{28}$$

The bound is attained when $\widetilde{\mathbf{W}}_{BB}[k]$ comprises the N_s principal left singular vectors of $\mathbf{U}_W^* \mathbf{W}[k]$, for each k, so that such choice is optimal. Then problem (27) reduces to

$$\max_{\mathbf{U}_W} J_W(\mathbf{U}_W) \triangleq \frac{1}{K} \sum_{k=0}^{K-1} \sum_{i=1}^{N_s} \lambda_i \left(\mathbf{U}_W^* \mathbf{W}[k] \mathbf{W}^*[k] \mathbf{U}_W \right) \tag{29}$$
$$\text{s. to } \mathbf{U}_W^* \mathbf{U}_W = \mathbf{I}_{L_r}.$$

The exact solution to (29) is not known unless $L_r = N_s$. To find an approximate solution for the general case $L_r \geq N_s$, the following result is useful; see Appendix C for the proof.

Proposition 1. *For any semi-unitary $\mathbf{U}_W \in \mathbb{C}^{N_r \times L_r}$, the cost $J_W(\mathbf{U}_W)$ can be bounded as*

$$\sum_{i=1}^{N_s} \lambda_i \left(\mathbf{U}_W^* \mathbf{S} \mathbf{U}_W \right) \leq J_W(\mathbf{U}_W) \leq \text{tr}\{\mathbf{U}_W^* \mathbf{S} \mathbf{U}_W\}, \tag{30}$$

where

$$\mathbf{S} \triangleq \frac{1}{K} \sum_{k=0}^{K-1} \mathbf{W}[k] \mathbf{W}^*[k] \tag{31}$$

is the average of the orthogonal projection matrices corresponding to the all-digital combiners for the different subcarriers[2].

Applying Poincaré separation theorem [37, p. 248], one has that (i) the upper bound in (30) is maximized when the columns of $\mathbf{U}_W$ comprise the L_r principal eigenvectors of $\mathbf{S}$; and (ii) the lower bound in (30) is maximized when N_s of the columns of $\mathbf{U}_W$ comprise the N_s principal eigenvectors of $\mathbf{S}$; the remaining $L_r - N_s$ columns are irrelevant as long as $\mathbf{U}_W^* \mathbf{U}_W = \mathbf{I}_{L_r}$ holds. Hence, choosing $\mathbf{U}_W$ as the L_r principal eigenvectors of $\mathbf{S}$ simultaneously maximizes *both* upper and lower bounds, providing a sensible approximate solution to (29). Note that if $L_r = N_s$ this solution becomes exact, since both bounds in (30) hold with equality. Thus, denoting such

[2]Note that $\mathbf{S}$ is not a projection matrix itself [36].

Algorithm 2 Hybrid combiner design

Input: All-digital combiners $\{\mathbf{W}[k]\}_{k=0}^{K-1}$
Compute $\mathbf{S} = \frac{1}{K} \sum_{k=0}^{K-1} \mathbf{W}[k] \mathbf{W}^*[k]$
Set $\mathbf{U}_S \leftarrow L_r$ principal eigenvectors of $\mathbf{S}$
Project $\mathbf{U}_S$ to obtain $\mathbf{W}_{RF}$ as per (32)
Perform SVD $\mathbf{W}_{RF} = \mathbf{U}_W \boldsymbol{\Sigma}_W \mathbf{V}_W^*$
for $k = 0, \ldots, K - 1$ **do**
    Set $\widetilde{\mathbf{W}}_{BB}[k] \leftarrow N_s$ principal left singular vectors of $\mathbf{U}_W^* \mathbf{W}[k]$
    Set $\mathbf{W}_{BB}[k] \leftarrow \mathbf{V}_W \boldsymbol{\Sigma}_W^{-1} \widetilde{\mathbf{W}}_{BB}[k]$
end for
Output: RF combiner $\mathbf{W}_{RF}$, baseband combiners $\{\mathbf{W}_{BB}[k]\}_{k=0}^{K-1}$

---

eigenvectors by $\mathbf{U}_S \in \mathbb{C}^{N_r \times L_r}$, we choose the RF combiner as its projection onto $\mathcal{M}_{b_r}^{N_r \times L_r}$, i.e.,

$$[\mathbf{W}_{RF}]_{p,q} = \exp(j Q\{\angle(\mathbf{e}_p^* \mathbf{U}_S \mathbf{e}_q); b_r\}), \begin{cases} 1 \leq p \leq N_r, \\ 1 \leq q \leq L_r, \end{cases} \tag{32}$$

where $Q\{\cdot; b\}$ denotes the phase quantization operation with b bits. With this value of $\mathbf{W}_{RF}$, with SVD $\mathbf{W}_{RF} = \mathbf{U}_W \boldsymbol{\Sigma}_W \mathbf{V}_W^*$, the baseband combiners are finally obtained as follows. Let the columns of $\mathbf{R}[k]$ comprise the N_s principal left singular vectors of $\mathbf{U}_W^* \mathbf{W}[k]$; then, we set $\mathbf{W}_{BB}[k] = \mathbf{V}_W \boldsymbol{\Sigma}_W^{-1} \mathbf{R}[k]$, $k = 0, 1, \ldots, K - 1$.

The hybrid combiner design is summarized in Algorithm 2. For given all-digital combiners, its computational complexity is $O(K N_r^2 N_s)$, as it is dominated by the computation of $\mathbf{S}$ in (31).

B. Direct approximation of combiners

In this approach, the hybrid combiner is the solution to

$$\min_{\mathbf{W}_{RF}, \{\mathbf{W}_{BB}[k]\}} \sum_{k=0}^{K-1} \| \mathbf{W}[k] - \mathbf{W}_{RF} \mathbf{W}_{BB}[k] \|_F^2 \tag{33}$$
$$\text{s. to} \begin{cases} \mathbf{W}_{RF} \in \mathcal{M}_{b_r}^{N_r \times L_r}, \\ (\mathbf{W}_{RF} \mathbf{W}_{BB}[k])^* (\mathbf{W}_{RF} \mathbf{W}_{BB}[k]) = \mathbf{I}_{N_s} \; \forall k. \end{cases}$$

Defining the matrices $\mathbf{W} \in \mathbb{C}^{N_r \times K N_s}$ and $\mathbf{W}_{BB} \in \mathbb{C}^{L_r \times K N_s}$ as

$$\mathbf{W} \triangleq \begin{bmatrix} \mathbf{W}[0] & \mathbf{W}[1] & \cdots & \mathbf{W}[K-1] \end{bmatrix}, \tag{34}$$
$$\mathbf{W}_{BB} \triangleq \begin{bmatrix} \mathbf{W}_{BB}[0] & \mathbf{W}_{BB}[1] & \cdots & \mathbf{W}_{BB}[K-1] \end{bmatrix} \tag{35}$$

the cost in (33) can be rewritten as $\| \mathbf{W} - \mathbf{W}_{RF} \mathbf{W}_{BB} \|_F^2$. Since in practice one has $L_r < K N_s$, problem (33) can be interpreted as one of finding a low-rank approximant $\mathbf{W}_{RF} \mathbf{W}_{BB}$ (with rank L_r) of the matrix $\mathbf{W}$, with additional hardware-related and semi-unitary constraints. Momentarily ignoring those constraints, the optimal factor $\mathbf{W}_{RF}$ can be chosen as the L_r principal left singular vectors of $\mathbf{W}$, by virtue of the Eckart-Young theorem [38]; or equivalently, and recalling (31), as the L_r principal eigenvectors of $\mathbf{W} \mathbf{W}^* = K \mathbf{S}$. Projecting these onto $\mathcal{M}_{b_r}^{N_r \times L_r}$, we obtain the same RF combiner as in (32). For this

choice, with the SVD $\mathbf{W}_{\text{RF}} = \mathbf{U}_W \mathbf{\Sigma}_W \mathbf{V}_W^*$, and letting again $\widetilde{\mathbf{W}}_{\text{BB}}[k] \triangleq \mathbf{\Sigma}_W \mathbf{V}_W^* \mathbf{W}_{\text{BB}}[k]$, the problem reduces to

$$\min_{\{\widetilde{\mathbf{W}}_{\text{BB}}[k]\}} \sum_{k=0}^{K-1} \left\| \mathbf{W}[k] - \mathbf{U}_W \widetilde{\mathbf{W}}_{\text{BB}}[k] \right\|_F^2 \tag{36}$$
$$\text{s. to } \widetilde{\mathbf{W}}_{\text{BB}}^*[k]\widetilde{\mathbf{W}}_{\text{BB}}[k] = \mathbf{I}_{N_s} \ \forall k,$$

which is decoupled across the K subcarriers, and is recognized as a generalization[3] of the orthogonal Procrustes problem [39, p. 601]. Considering the SVD $\mathbf{U}_W^* \mathbf{W}[k] = \mathbf{R}[k]\mathbf{\Sigma}[k]\mathbf{V}^*[k]$, the solution is given by $\widetilde{\mathbf{W}}_{\text{BB}}[k] = \mathbf{R}[k]\mathbf{V}^*[k]$ for all k, matching the solution obtained in Sec. V-A up to the $N_s \times N_s$ unitary matrix $\mathbf{V}^*[k]$, which does not affect the spectral efficiency. This lends additional justification to the hybrid combiner design of Algorithm 2.

VI. Design of frequency-selective hybrid precoders

We focus now on the frequency-selective hybrid precoders $\mathbf{F}_{\text{RF}}\mathbf{F}_{\text{BB}}[k]$ under the per-antenna or per-RF chain power constraints. Since the spectral efficiency (9) depends on the all-digital precoder only through the matrices[4] $\mathbf{F}[k]\mathbf{F}^*[k]$, one may attemp to match these, such that $\mathbf{F}_{\text{RF}}\mathbf{F}_{\text{BB}}[k](\mathbf{F}_{\text{RF}}\mathbf{F}_{\text{BB}}[k])^* \approx \mathbf{F}[k]\mathbf{F}^*[k]$. But in view of our findings in Sec. V, direct approximation of the all-digital precoders $\mathbf{F}_{\text{RF}}\mathbf{F}_{\text{BB}}[k] \approx \mathbf{F}[k]$ may be expected to provide similar results, so we adopt this latter approach in the sequel.

A. Analog RF precoder

Let $\{\mathbf{F}[k]\}$ be the frequency-selective all-digital precoder obtained in Sec. IV, either under uniform or non-uniform power allocation. Defining the matrices $\mathbf{F} \in \mathbb{C}^{N_t \times KN_s}$ and $\mathbf{F}_{\text{BB}} \in \mathbb{C}^{L_t \times KN_s}$ as

$$\mathbf{F} \triangleq \begin{bmatrix} \mathbf{F}[0] & \mathbf{F}[1] & \cdots & \mathbf{F}[K-1] \end{bmatrix}, \tag{37}$$
$$\mathbf{F}_{\text{BB}} \triangleq \begin{bmatrix} \mathbf{F}_{\text{BB}}[0] & \mathbf{F}_{\text{BB}}[1] & \cdots & \mathbf{F}_{\text{BB}}[K-1] \end{bmatrix}, \tag{38}$$

the corresponding problem becomes one of low-rank approximation with additional constraints:

$$\min_{\mathbf{F}_{\text{RF}}, \mathbf{F}_{\text{BB}}} \|\mathbf{F} - \mathbf{F}_{\text{RF}}\mathbf{F}_{\text{BB}}\|_F^2$$
$$\text{s. to } \begin{cases} \mathbf{F}_{\text{RF}} \in \mathcal{M}_{b_t}^{N_t \times L_t}, \\ \frac{1}{KN_s}\mathbf{e}_j^* \mathbf{F}_{\text{RF}}\mathbf{F}_{\text{BB}}\mathbf{F}_{\text{BB}}^*\mathbf{F}_{\text{RF}}^*\mathbf{e}_j \leq \bar{p}_j, \forall j \quad \text{(per-antenna)}, \\ \text{or } \frac{1}{KN_s}\mathbf{e}_\ell^* \mathbf{F}_{\text{BB}}\mathbf{F}_{\text{BB}}^*\mathbf{e}_\ell \leq \bar{q}_\ell, \forall \ell \quad \text{(per-RF chain)}. \end{cases} \tag{39}$$

Momentarily ignoring the constraints, we may invoke the Eckart-Young theorem as in Sec. V-B to select the left factor in the approximant as the L_t principal left singular vectors of $\mathbf{F}$, or equivalently as the L_t principal eigenvectors of

$$\mathbf{T} \triangleq \frac{1}{K}\mathbf{F}\mathbf{F}^* = \frac{1}{K}\sum_{k=0}^{K-1} \mathbf{F}[k]\mathbf{F}^*[k]. \tag{40}$$

[3]Since the variable is only semi-unitary and not necessarily unitary.

[4]With non-uniform power allocation across subcarriers and data streams, $\mathbf{F}[k]$ is not semi-unitary, so that $\mathbf{F}[k]\mathbf{F}^*[k]$ is not an orthogonal projection matrix.

Thus, we set the RF precoder as the projection of such eigenvectors, say $\mathbf{U}_T \in \mathbb{C}^{N_t \times L_t}$, onto $\mathcal{M}_{b_t}^{N_t \times L_t}$, i.e.,

$$[\mathbf{F}_{\text{RF}}]_{p,q} = \exp(jQ\{\angle(\mathbf{e}_p^* \mathbf{U}_T \mathbf{e}_q); b_t\}), \quad \begin{cases} 1 \leq p \leq N_t, \\ 1 \leq q \leq L_t, \end{cases} \tag{41}$$

We note that, following a different route based on maximizing an approximation to the mutual information, the authors of [7] arrived at a similar design for the RF precoder, in which $\mathbf{F}[k]$ is replaced in (40) by the N_s dominant singular vectors of the channel matrix $\mathbf{H}[k]$.

B. Digital baseband precoder

Once $\mathbf{F}_{\text{RF}}$ is fixed, it remains to obtain the baseband factor $\mathbf{F}_{\text{BB}}$ taking the power constraints into account. Developing the objective in (39) yields

$$\begin{aligned} \|\mathbf{F} - \mathbf{F}_{\text{RF}}\mathbf{F}_{\text{BB}}\|_F^2 &= \|\mathbf{F}\|_F^2 + \|\mathbf{F}_{\text{RF}}\mathbf{F}_{\text{BB}}\|_F^2 \\ &\quad - 2\,\text{Re}\,\text{tr}\left\{\mathbf{F}^*\mathbf{F}_{\text{RF}}\mathbf{F}_{\text{BB}}\right\}. \end{aligned} \tag{42}$$

In the case of per-antenna power constraints, if these are all met with equality, then $\|\mathbf{F}_{\text{RF}}\mathbf{F}_{\text{BB}}\|_F^2 = KN_s \sum_{j=1}^{N_t} \bar{p}_j$, and the dependence on $\mathbf{F}_{\text{BB}}$ of (42) is through the last term only. In the case of per-RF chain power constraints, we argue that this is also approximately true. Recall that the analog precoder satisfies $\mathbf{F}_{\text{RF}}^*\mathbf{F}_{\text{RF}} \approx N_t\mathbf{I}_{L_t}$ with high probability [10, Lemma 1], so that

$$\begin{aligned} \|\mathbf{F}_{\text{RF}}\mathbf{F}_{\text{BB}}\|_F^2 &= \text{tr}\left\{\mathbf{F}_{\text{BB}}^*\mathbf{F}_{\text{RF}}^*\mathbf{F}_{\text{RF}}\mathbf{F}_{\text{BB}}\right\} \\ &\approx N_t\,\text{tr}\left\{\mathbf{F}_{\text{BB}}^*\mathbf{F}_{\text{BB}}\right\} \\ &= N_t\,\text{tr}\left\{\mathbf{F}_{\text{BB}}\mathbf{F}_{\text{BB}}^*\right\}, \end{aligned} \tag{43}$$

which equals $N_t KN_s \sum_{\ell=1}^{L_t} \bar{q}_\ell$ if the per-RF chain power constraints are met with equality. Hence, we propose to focus on the minimization of the last term in (42).

Introducing $\mathbf{G} = \mathbf{F}_{\text{RF}}^*\mathbf{F} \in \mathbb{C}^{L_t \times KN_s}$ and the SVD $\mathbf{F}_{\text{BB}} = \mathbf{U}_{\text{BB}}\mathbf{\Sigma}_{\text{BB}}\mathbf{V}_{\text{BB}}^*$, where $\mathbf{U}_{\text{BB}} \in \mathbb{C}^{L_t \times L_t}$, $\mathbf{\Sigma}_{\text{BB}} \in \mathbb{C}^{L_t \times L_t}$, and $\mathbf{V}_{\text{BB}} \in \mathbb{C}^{KN_s \times L_t}$, the problem becomes

$$\max_{\mathbf{U}_{\text{BB}}, \mathbf{\Sigma}_{\text{BB}}, \mathbf{V}_{\text{BB}}} \text{Re}\,\text{tr}\left\{\mathbf{G}^*\mathbf{U}_{\text{BB}}\mathbf{\Sigma}_{\text{BB}}\mathbf{V}_{\text{BB}}^*\right\}$$
$$\text{s. to } \begin{cases} \mathbf{U}_{\text{BB}}^*\mathbf{U}_{\text{BB}} = \mathbf{I}_{L_t}, \quad \mathbf{V}_{\text{BB}}^*\mathbf{V}_{\text{BB}} = \mathbf{I}_{L_t}, \\ \frac{1}{KN_s}\mathbf{e}_j^*\mathbf{F}_{\text{RF}}\mathbf{U}_{\text{BB}}\mathbf{\Sigma}_{\text{BB}}^2\mathbf{U}_{\text{BB}}^*\mathbf{F}_{\text{RF}}^*\mathbf{e}_j \leq \bar{p}_j, \forall j \quad \text{(per-antenna)}, \\ \text{or } \frac{1}{KN_s}\mathbf{e}_\ell^*\mathbf{U}_{\text{BB}}\mathbf{\Sigma}_{\text{BB}}^2\mathbf{U}_{\text{BB}}^*\mathbf{e}_\ell \leq \bar{q}_\ell, \forall \ell \quad \text{(per-RF chain)}. \end{cases} \tag{44}$$

Solving (44) is difficult due to the fact that $\mathbf{U}_{\text{BB}}$ affects the power constraints. Similarly to Sec. IV, we adopt an approach by which we first optimize the semi-unitary matrices $\mathbf{U}_{\text{BB}}$, $\mathbf{V}_{\text{BB}}$ neglecting the power constraints, and then optimize $\mathbf{\Sigma}_{\text{BB}}$ under the power constraints. The solution thus obtained is feasible for (44), but not necessarily optimal. Hence, we must first solve

$$\max_{\mathbf{U}_{\text{BB}}, \mathbf{V}_{\text{BB}}} \text{Re}\,\text{tr}\left\{\mathbf{G}^*\mathbf{U}_{\text{BB}}\mathbf{\Sigma}_{\text{BB}}\mathbf{V}_{\text{BB}}^*\right\}$$
$$\text{s. to } \mathbf{U}_{\text{BB}}^*\mathbf{U}_{\text{BB}} = \mathbf{I}_{L_t}, \quad \mathbf{V}_{\text{BB}}^*\mathbf{V}_{\text{BB}} = \mathbf{I}_{L_t}. \tag{45}$$

Consider now the SVD $\mathbf{G} = \mathbf{U}_G \mathbf{\Sigma}_G \mathbf{V}_G^*$. Assuming that the singular values in $\mathbf{\Sigma}_G$ and $\mathbf{\Sigma}_{\text{BB}}$ are in decreasing order, application of Von Neumann's trace inequality reveals that the solution to (45) is given by $\mathbf{U}_{\text{BB}} = \mathbf{U}_G$ and $\mathbf{V}_{\text{BB}} = \mathbf{V}_G$. After

This article has been accepted for publication in IEEE Transactions on Wireless Communications. This is the author's version which has not been fully edited and content may change prior to final publication. Citation information: DOI 10.1109/TWC.2022.3142959

9

Algorithm 3 Hybrid precoder design under per-antenna or per-RF chain power constraints

---

Input: All-digital precoders $\{\mathbf{F}[k]\}_{k=0}^{K-1}$, available powers $\{\bar{p}_j\}_{j=1}^{N_\mathrm{t}}$ or $\{\bar{q}_\ell\}_{\ell=1}^{L_\mathrm{t}}$
Compute $\mathbf{T} = \frac{1}{K} \sum_{k=0}^{K-1} \mathbf{F}[k]\mathbf{F}^*[k]$
Set $\mathbf{U}_T \leftarrow L_\mathrm{t}$ principal eigenvectors of $\mathbf{T}$
Project $\mathbf{U}_T$ to obtain $\mathbf{F}_{\mathrm{RF}}$ as per (41)
Compute $\mathbf{G} = \mathbf{F}_{\mathrm{RF}}^* \begin{bmatrix} \mathbf{F}[0] & \cdots & \mathbf{F}[K-1] \end{bmatrix}$
Perform SVD $\mathbf{G} = \mathbf{U}_G \mathbf{\Sigma}_G \mathbf{V}_G^*$
Non-uniform power alloc.: Solve for $\mathbf{\Sigma}_{\mathrm{BB}}$ in (46)
Uniform power alloc.: Compute (47) and set $\mathbf{\Sigma}_{\mathrm{BB}} = \sigma_{\mathrm{BB}}\mathbf{I}_{L_\mathrm{t}}$
Set $\begin{bmatrix} \mathbf{F}_{\mathrm{BB}}[0] & \cdots & \mathbf{F}_{\mathrm{BB}}[K-1] \end{bmatrix} = \mathbf{U}_G \mathbf{\Sigma}_{\mathrm{BB}} \mathbf{V}_G^*$
Output: RF precoder $\mathbf{F}_{\mathrm{RF}}$, baseband precoders $\{\mathbf{F}_{\mathrm{BB}}[k]\}_{k=0}^{K-1}$

---

substituting these in (44), it remains to maximize $\mathrm{tr}\{\mathbf{\Sigma}_G \mathbf{\Sigma}_{\mathrm{BB}}\}$ w.r.t. $\mathbf{\Sigma}_{\mathrm{BB}}$ subject to the power constraints, i.e.,

$$
\begin{aligned}
\max_{\{\sigma_{\mathrm{BB},\ell}\}} \quad & \sum_{\ell=1}^{L_\mathrm{t}} \sigma_{G,\ell}\sigma_{\mathrm{BB},\ell} \\
\text{s. to} \quad & \begin{cases} \sigma_{\mathrm{BB},1} \geq \sigma_{\mathrm{BB},2} \geq \cdots \geq \sigma_{\mathrm{BB},L_\mathrm{t}} \geq 0, \\ \frac{1}{KN_\mathrm{s}} \sum_{\ell=1}^{L_\mathrm{t}} \left|\mathbf{e}_\ell^*\mathbf{U}_G^*\mathbf{F}_{\mathrm{RF}}^*\mathbf{e}_j\right|^2 \sigma_{\mathrm{BB},\ell}^2 \leq \bar{p}_j, \forall j \quad \text{(per-antenna)}, \\ \text{or} \quad \frac{1}{KN_\mathrm{s}} \sum_{\ell=1}^{L_\mathrm{t}} \left|\mathbf{e}_\ell^*\mathbf{U}_G^*\mathbf{e}_{\ell'}\right|^2 \sigma_{\mathrm{BB},\ell}^2 \leq \bar{q}_{\ell'}, \forall \ell' \quad \text{(per-RF chain)}. \end{cases}
\end{aligned}
\tag{46}
$$

Note that the singular values $\{\sigma_{\mathrm{BB},\ell}\}_{\ell=1}^{L_\mathrm{t}}$ can be interpreted as power allocation coefficients *at the transmit RF chain level*.

Problem (46) has a linear objective and convex quadratic constraints, so it can be expressed as a second-order cone program (SOCP). Although the number of variables, L_t, is relatively small, a suboptimal solution that avoids having to solve an SOCP altogether is obtained by imposing $\sigma_{\mathrm{BB},\ell} = \sigma_{\mathrm{BB}}$ for all ℓ. In that case, the optimal value is readily found to be

$$
\sigma_{\mathrm{BB}} = \begin{cases} \sqrt{\frac{KN_\mathrm{s}}{L_\mathrm{t}} \min_{1 \leq j \leq N_\mathrm{t}}\{\bar{p}_j\}} & \text{(per-antenna)}, \\ \sqrt{KN_\mathrm{s} \min_{1 \leq \ell \leq L_\mathrm{t}}\{\bar{q}_\ell\}} & \text{(per-RF chain)}, \end{cases}
\tag{47}
$$

where we have used the fact that $\sum_{\ell=1}^{L_\mathrm{t}} \left|\mathbf{e}_\ell^*\mathbf{U}_G^*\mathbf{F}_{\mathrm{RF}}^*\mathbf{e}_j\right|^2 = L_\mathrm{t}$ for all j, since the entries of $\mathbf{F}_{\mathrm{RF}}$ have unit modulus and $\mathbf{U}_G$ is unitary; similarly, $\sum_{\ell=1}^{L_\mathrm{t}} \left|\mathbf{e}_\ell^*\mathbf{U}_G^*\mathbf{e}_{\ell'}\right|^2 = 1$ for all ℓ'. With this choice, it is readily seen that in the case of per-antenna power constraints, all antennas transmit with the same power $p_0 \triangleq \min_{1 \leq j \leq N_\mathrm{t}}\{p_j\}$; and in the case of per-RF chain power constraints, all RF chains deliver the same power $q_0 \triangleq \min_{1 \leq \ell \leq L_\mathrm{t}}\{q_\ell\}$. Thus, in the important case of uniform power constraints (i.e., $p_j = p_0 \,\forall j$, or $q_\ell = q_0 \,\forall \ell$), this design guarantees that all constraints are satisfied with equality. This is true regardless of the resolution of analog phase-shifters.

The hybrid precoder design is summarized in Algorithm 3. For given all-digital precoders, its complexity is $O(KN_\mathrm{t}^2 N_\mathrm{s})$, as it is mainly due to the computation of $\mathbf{T}$ in (40). Thus, since $N_\mathrm{s} \ll \min(N_\mathrm{t}, N_\mathrm{r})$, the overall complexity of the complete hybrid design is dominated by the initial computation of the all-digital matrices, which is $O(K \min(N_\mathrm{t}^2 N_\mathrm{r}, N_\mathrm{r}^2 N_\mathrm{t}))$ assuming uniform power allocation (see Sec. IV).
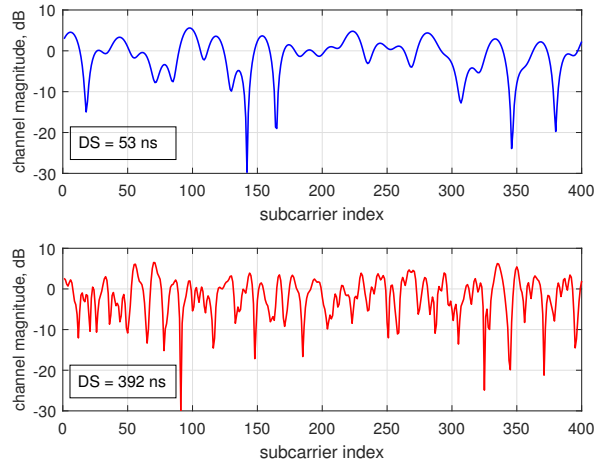

Fig. 2: Frequency response of two channel realizations between a TX-RX antenna pair. Scenario I, $K_R = 0$ dB. Delay spread = 53 ns (top) and 392 ns (bottom).

VII. NUMERICAL RESULTS

A. Scenario description

Simulation results are presented for a mmWave MIMO system with a bandwidth $B = 200$ MHz operating at a carrier frequency $f_\mathrm{c} = 50$ GHz. Both transmitter and receiver are equipped with half-wavelength Uniform Linear Arrays (ULAs). The number of active subcarriers is $K = 400$, with cyclic prefix length $Z_{\mathrm{CP}} = 100$. Thus, the subcarrier spacing is $\Delta_f = \frac{B}{K} = 500$ kHz, the temporal duration of the useful part of the OFDM symbol is $\frac{1}{\Delta_f} = 2\ \mu$s, and the guard interval is $\frac{Z_{\mathrm{CP}}}{K\Delta_f} = 500$ ns. The pulse shaping filter accounting for filtering effects at the transmitter and receiver is a raised cosine filter with 25% excess bandwidth. The mmWave frequency-selective channel is generated according to (2) using small-scale fading parameters generated with the QuaDRiGa channel simulator [40], [41] following the 3GPP TR 38.901 Urban Macrocell (UMa) scenario as specified in [27], with maximum delay spread of 500 ns as suggested in [42]. The influence of the MIMO channel Rician factor, denoted as K_R, will also be illustrated. Results are averaged over 100 independent channel realizations. We consider two different setups:

- Scenario I: the number of transmit and receive antennas are $N_\mathrm{t} = 64$, $N_\mathrm{r} = 32$, and the number of RF chains is set to $L_\mathrm{t} = 4$, $L_\mathrm{r} = 4$.
- Scenario II: the number of transmit and receive antennas are $N_\mathrm{t} = 64$, $N_\mathrm{r} = 16$, and the number of RF chains is set to $L_\mathrm{t} = 4$, $L_\mathrm{r} = 2$.

Fig. 2 shows two typical channel responses, confirming the frequency selectivity of this setting.

B. All-digital design

First we evaluate the performance of the all-digital design of Sec. IV. As a benchmark we consider a standard design with a total power constraint (TPC) P, in which precoders and combiners are taken from the dominant singular vectors of the
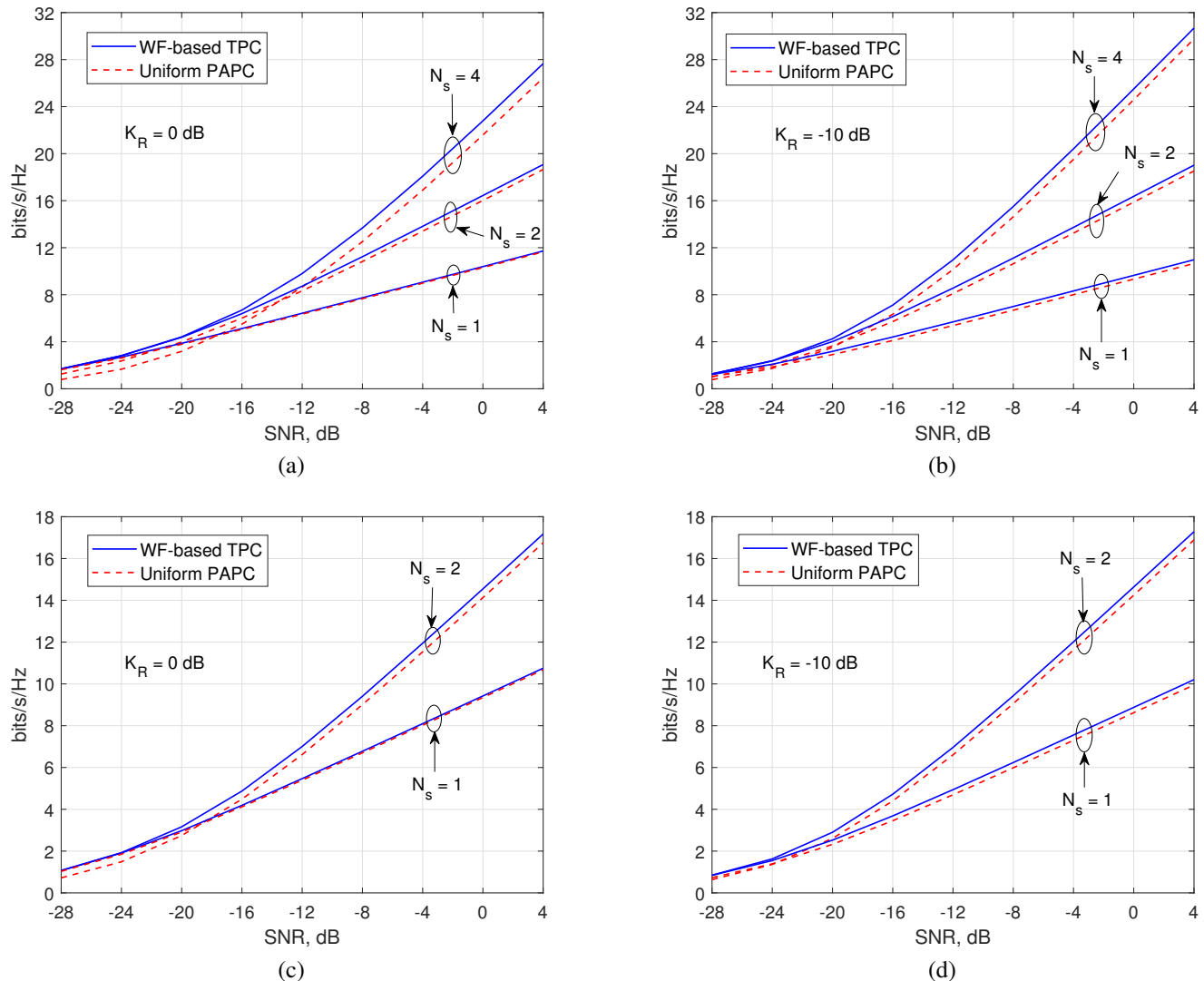
Fig. 3: Spectral efficiency vs. SNR for all-digital designs. (a) Scenario I, $K_R = 0$ dB; (b) Scenario I, $K_R = -10$ dB; (c) Scenario II, $K_R = 0$ dB; (d) Scenario II, $K_R = -10$ dB.

channel matrices $\mathbf{H}[k]$, with optimal power allocation obtained via waterfilling (WF). For the design with per-antenna power constraints (PAPC) we assume equal constraints $p_j = P/N_t$ across antennas, so that the total transmit power is P for both designs. Results for Scenarios I and II and Rician factor values of 0 and -10 dB are shown in Fig. 3, with the PAPC design following the uniform power allocation in (23). It is seen that the gap between this PAPC design with uniform power allocation and the WF-based TPC design remains small, although it increases with the number of data streams N_s. The spectral efficiency of the optimal space-frequency power allocation strategy (21) lies between these two, showing that the simple uniform power allocation approach of (23) provides a very good tradeoff between performance and complexity. Fig. 3 also shows that the Rician factor has no significant impact on performance; this is likely due to the fact that the proposed designs do not rely on any particular channel structure.

C. Hybrid design

Figs. 4 and 5 show the performance of the proposed hybrid designs under Scenarios I and II, respectively, considering both per-antenna (PAPC) and per-RF chain (PRFPC) power constraints. The all-digital precoders and combiners used as reference for the hybrid designs were obtained as per Algorithm 1 with uniform power allocation. Equal power constraints were imposed on the hybrid designs, i.e., $p_j = P/N_t$, $j = 1, \dots, N_t$ for PAPC and $q_\ell = P/(L_t N_t)$, $\ell = 1, \dots, L_t$ for PRFPC. The hybrid combiners were computed as in Algorithm 2, whereas for the hybrid precoders we considered both uniform (UPA) and non-uniform (NUPA) power allocation versions of Algorithm 3. The same bit resolution is assumed for the phase shifters at the transmitter and receiver, i.e., $b_t = b_r$.

For PAPC, it is seen that the NUPA approach provides a slight improvement with respect to UPA, but this advantage diminishes as the number of data streams increases; for example, in Scenario I with $N_s = 4$, cf. Fig. 4(a), there is virtually
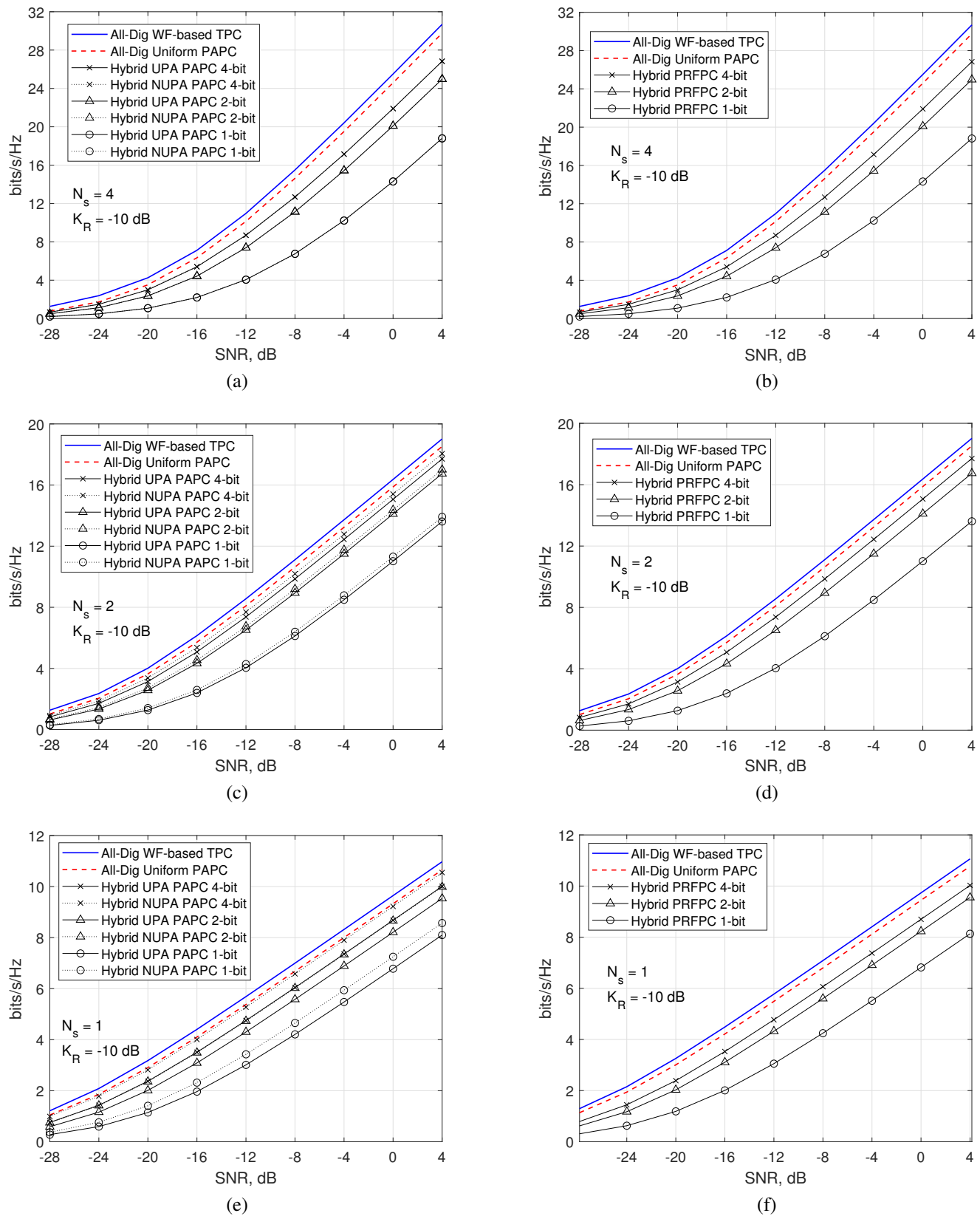
Fig. 4: Spectral efficiency vs. SNR. Scenario I, $K_R = -10$ dB. Left: Per-Antenna Power Constraints; Right: Per-RF Chain Power Constraints. Top: $N_s = 4$; Middle: $N_s = 2$; Bottom: $N_s = 1$.
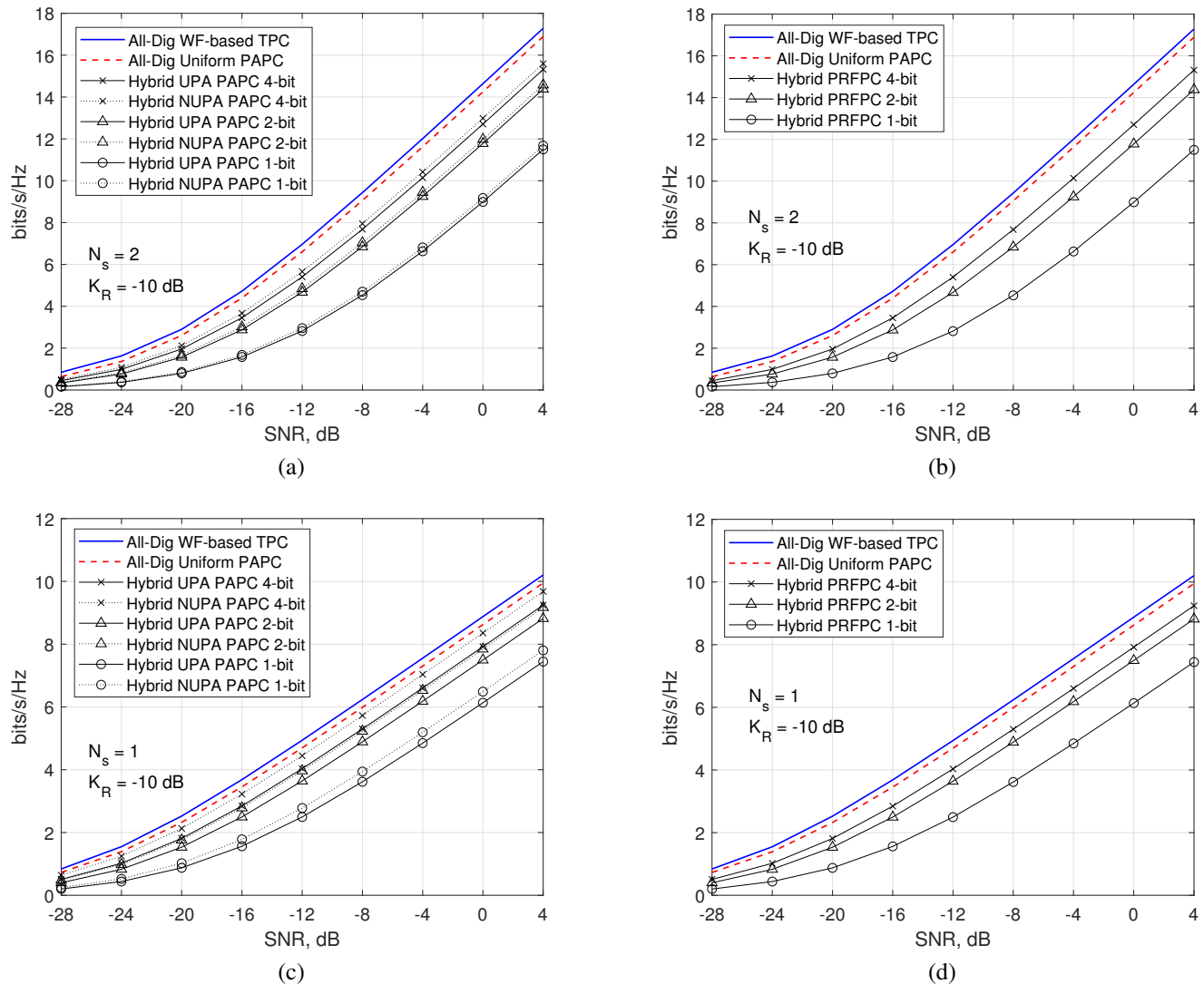
Fig. 5: Spectral efficiency vs. SNR. Scenario II, $K_R = -10$ dB. Left: Per-Antenna Power Constraints; Right: Per-RF Chain Power Constraints. Top: $N_s = 2$; Bottom: $N_s = 1$.

no difference in performance between the two approaches. For PRFPC, the results of UPA and NUPA are indistinguishable in all cases.

The loss in performance for PAPC with respect to the all-digital reference design due to finite-resolution phase shifters becomes more pronounced with a larger number of data streams. For $N_s = 1$, and with $b_t = b_r = 4$ bits, the spectral efficiency of the hybrid NUPA design is very close to that of the all-digital reference in both scenarios. In Scenario I with $N_s = 4$, a loss of 2, 4 and 8 dB is respectively observed with 4-, 2- and 1-bit resolution phase shifters. Regarding PRFPC, it is seen that its performance is very similar to that of UPA-PAPC for all cases. Note that even with very coarse quantization, the spatial multiplexing gain of the all-digital design is achieved, i.e., the spectral efficiency vs. SNR curves present the same slope, under either PAPC or PRFPC.

The complementary cumulative distribution function (CCDF) of the power delivered to any given antenna under

TPC and PAPC designs is shown in Fig. 6. On the one hand, the hybrid UPA-PAPC design is seen to meet the power constraints with equality, as expected from the remarks following (47). On the other hand, although both the all-digital PAPC and the hybrid NUPA-PAPC designs always satisfy the per-antenna power constraints, these are not necessarily met with equality. Therefore, there may be antennas whose amplifiers do not deliver their maximum available power, although the probability of this event decreases with larger number of data streams. For example, in the setting of Fig. 6(a) (Scenario I), with the hybrid NUPA-PAPC design (4-bit phase shifter resolution) the percentage of amplifiers within 0.5 dB of their maximum power output are 62%, 86.5% and 100% respectively for $N_s = 1$, 2 and 4. Note that, in view of Lemma 1, the fact that the all-digital PAPC design does not meet the power constraints with equality indicates that this design is suboptimal with respect to Problem (16), due to the approximations introduced in Sec. IV. Interestingly,
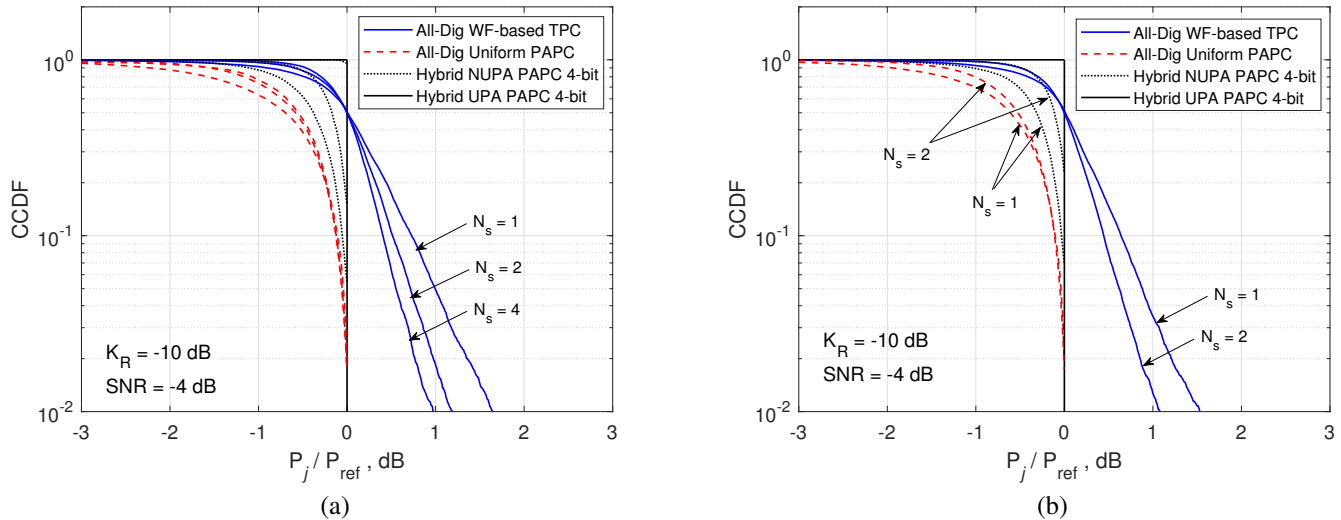
This article has been accepted for publication in IEEE Transactions on Wireless Communications. This is the author's version which has not been fully edited and content may change prior to final publication. Citation information: DOI 10.1109/TWC.2022.3142959

13

Fig. 6: CCDF of the different designs. SNR = −4 dB, K_R = −10 dB. (a) Scenario I; (b) Scenario II. The reference power is defined as $P_{\mathrm{ref}} = P/N_{\mathrm{t}}$.

the hybrid PAPC designs yield larger delivered power to any given antenna than the all-digital PAPC design, so that the performance loss ensuing from the hardware constraints of the hybrid architecture is partially compensated by an increase in transmit power, whenever this is feasible.

In contrast, the all-digital WF-based TPC design violates the per-antenna power constraints, resulting in larger power spread across antennas for smaller values of N_s. For example, under Scenario I, i.e., Fig. 6(a), if a probability of 0.01 for a given antenna not fulfilling the power constraint is desired, the transmit power would have to be backed off by approximately 1.7, 1.2 and 1 dB for N_s = 1, 2 and 4 respectively. Thereby, the corresponding spectral efficiency curves for WF-based TPC in Fig. 4 would need to be shifted to the right by these same amounts. This clearly shows the importance of considering adequate power constraints in the design of practical mmWave MIMO systems.

VIII. Conclusions

We considered the design of precoders and combiners for frequency-selective mmWave channels under a multicarrier approach, and adopting per-antenna or per-RF chain power constraints, which are more realistic than the total power constraint usually found in the literature. When hybrid architectures are considered, the pivotal point of the design is the determination of the analog term in the corresponding factorization, which is common to all subcarriers. We posed the corresponding problem as one of subspace approximation, for which accurate suboptimal solutions were proposed, offering different tradeoffs in terms of performance and complexity. The influence of different system parameters on final performance was also analyzed, both in terms of spectral efficiency and power delivered to any given antenna, showing that the proposed design performs well even under low resolution of the phase shifters comprising the analog factors.

Although we have considered a single-user MIMO system, the proposed design can also be applied with straightforward modifications to an Orthogonal Frequency Division Multiple Access (OFDMA) multiuser MIMO system, in which the different users are scheduled over disjoint subsets of the available subcarriers. The case in which all users are scheduled simultaneously over the whole frequency band is significantly more challenging and is left for future work.

APPENDIX A
PROOF OF LEMMA 1

Let $\{\mathbf{W}_\star[k]\}_{k=0}^{K-1}$ be the combiner corresponding to the the solution of (16) and consider the SVD $\mathbf{W}_\star[k] = \mathbf{U}_\star[k]\mathbf{\Sigma}_\star[k]\mathbf{V}_\star^*[k]$. By fixing $\mathbf{W}[k] = \mathbf{W}_\star[k]$, the spectral efficiency becomes

$$\mathcal{R} = \frac{1}{K}\sum_{k=0}^{K-1}\log_2\left|\mathbf{I}_{N_s} + \frac{\mathrm{SNR}}{N_s}\mathbf{F}^*[k]\mathbf{H}^*[k]\mathbf{U}_\star[k]\mathbf{U}_\star^*[k]\mathbf{H}[k]\mathbf{F}[k]\right|,$$
(48)

corresponding to the mutual information for an effective channel $\hat{\mathbf{H}}[k] = \mathbf{U}_\star^*[k]\mathbf{H}[k]$. Then the result follows by applying analogous arguments to those in the proof of [18, Theorem 1]. Specifically, for a given $\ell \in \{0, 1, \ldots, K-1\}$, the objective (48), seen as a function of $\{\mathbf{F}[k]\}$, is written as the sum of two terms: the first one depends on the j-th row of $\mathbf{F}[\ell]$ only, and the second depends on the remaining rows of $\mathbf{F}[\ell]$ and on $\mathbf{F}[k]$ for $k \neq \ell$. Thus, it is seen that if the power constraint at the j-th antenna is not tight, then the j-th row of $\mathbf{F}[\ell]$ can be modified to improve the spectral efficiency while still meeting the constraints.

APPENDIX B
PROOF OF THEOREM 1

Since the optimization problem (18) is uncoupled across the K subcarriers, we neglect the subcarrier index k and, letting

$\gamma \triangleq \frac{\text{SNR}}{N_\text{s}}$, we focus on any one of the terms:

$$\max_{\{\mathbf{W}, \mathbf{U}_F\}} \mathcal{J} \triangleq \left| \mathbf{I}_{N_\text{s}} + \gamma \mathbf{W}\mathbf{W}^* \mathbf{H}\mathbf{U}_F \mathbf{\Sigma}_F^2 \mathbf{U}_F^* \mathbf{H}^* \right|$$
$$\text{s. to } \mathbf{W}^*\mathbf{W} = \mathbf{I}_{N_\text{s}}, \quad \mathbf{U}_F^*\mathbf{U}_F = \mathbf{I}_{N_\text{s}}. \tag{49}$$

Let $\mathbf{C} \triangleq \mathbf{H}\mathbf{U}_F \mathbf{\Sigma}_F^2 \mathbf{U}_F^* \mathbf{H}^*$, which is $N_\text{r} \times N_\text{r}$ positive semidefinite. Using [43, Lemma 3], $\mathcal{J}$ in (49) is upper bounded as

$$\begin{aligned}
\mathcal{J} &= \left| \mathbf{I}_{N_\text{s}} + \gamma \mathbf{W}\mathbf{W}^* \mathbf{C} \right| \\
&\leq \prod_{i=1}^{N_\text{r}} \left(1 + \gamma \lambda_i(\mathbf{W}\mathbf{W}^*) \lambda_i(\mathbf{C}) \right) \tag{50} \\
&= \prod_{i=1}^{N_\text{s}} \left(1 + \gamma \lambda_i(\mathbf{C}) \right) \triangleq \mathcal{J}_0, \tag{51}
\end{aligned}$$

since $\lambda_i(\mathbf{W}\mathbf{W}^*) = 1$ for $1 \leq i \leq N_\text{s}$ and zero otherwise. The upper bound in (51) is achieved if the columns of $\mathbf{W}$ comprise the N_s principal eigenvectors of $\mathbf{C}$.

Consider now maximizing $\mathcal{J}_0$ w.r.t. $\mathbf{U}_F$. The following bound applies:

$$\mathcal{J}_0 \leq \left| \mathbf{I}_{N_\text{r}} + \gamma \mathbf{C} \right| = \left| \mathbf{I}_{N_\text{s}} + \gamma \mathbf{U}_F \mathbf{\Sigma}_F^2 \mathbf{U}_F^* \mathbf{H}^* \mathbf{H} \right|. \tag{52}$$

Apply now [43, Lemma 3] to obtain

$$\begin{aligned}
\mathcal{J}_0 &\leq \prod_{i=1}^{N_\text{t}} \left(1 + \gamma \lambda_i(\mathbf{U}_F \mathbf{\Sigma}_F^2 \mathbf{U}_F^*) \lambda_i(\mathbf{H}^*\mathbf{H}) \right) \tag{53} \\
&= \prod_{i=1}^{N_\text{s}} \left(1 + \gamma \lambda_i(\mathbf{\Sigma}_F^2) \lambda_i(\mathbf{H}^*\mathbf{H}) \right), \tag{54}
\end{aligned}$$

since $\lambda_i(\mathbf{U}_F \mathbf{\Sigma}_F^2 \mathbf{U}_F^*) = \lambda_i(\mathbf{\Sigma}_F^2)$ for $1 \leq i \leq N_\text{s}$ and zero otherwise. Equality holds in (52) and (53) if the columns of $\mathbf{U}_F$ comprise the N_s principal right singular vectors of $\mathbf{H}$, and thus such $\mathbf{U}_F$ is optimal. In that case, the eigenvectors of $\mathbf{C} = \mathbf{H}\mathbf{U}_F \mathbf{\Sigma}_F^2 \mathbf{U}_F^* \mathbf{H}^*$ reduce to the left singular vectors of $\mathbf{H}$, and therefore the optimal $\mathbf{W}$ is given by the N_s principal left singular vectors.

APPENDIX C
PROOF OF PROPOSITION 1

The upper bound in (30) is derived as

$$\begin{aligned}
J_W(\mathbf{U}_W) &= \frac{1}{K} \sum_{k=0}^{K-1} \sum_{i=1}^{N_\text{s}} \lambda_i \left(\mathbf{U}_W^* \mathbf{W}[k] \mathbf{W}^*[k] \mathbf{U}_W \right) \\
&\leq \frac{1}{K} \sum_{k=0}^{K-1} \text{tr} \left\{ \mathbf{U}_W^* \mathbf{W}[k] \mathbf{W}^*[k] \mathbf{U}_W \right\} \\
&= \text{tr} \left\{ \mathbf{U}_W^* \left(\frac{1}{K} \sum_{k=0}^{K-1} \mathbf{W}[k] \mathbf{W}^*[k] \right) \mathbf{U}_W \right\} \\
&= \text{tr} \{ \mathbf{U}_W^* \mathbf{S} \mathbf{U}_W \}. \tag{55}
\end{aligned}$$

The lower bound in (30) follows by direct application of Ky Fan's eigenvalue inequality [37, Th. 4.3.47], which states that for Hermitian matrices $\mathbf{A}, \mathbf{B} \in \mathbb{C}^{n \times n}$, the vector of ordered eigenvalues of $\mathbf{A} + \mathbf{B}$ is majorized by the sum of those of $\mathbf{A}$ and $\mathbf{B}$, i.e., $\sum_{i=1}^{m} \lambda_i(\mathbf{A} + \mathbf{B}) \leq \sum_{i=1}^{m} [\lambda_i(\mathbf{A}) + \lambda_i(\mathbf{B})]$ for all $m \leq n$.

REFERENCES

[1] A. Alkhateeb, J. Mo, N. González-Prelcic, and R. W. Heath Jr., "MIMO precoding and combining solutions for millimeter-wave systems," *IEEE Commun. Mag.*, vol. 52, no. 12, pp. 122–131, Dec. 2014.

[2] X. Zhang, A. F. Molisch, and S.-Y. Kung, "Variable-phase-shift-based RF-baseband codesign for MIMO antenna selection," *IEEE Trans. Signal Process.*, vol. 53, no. 11, pp. 4091–4103, Nov. 2005.

[3] O. E. Ayach, S. Rajagopal, S. Abu-Surra, Z. Pi, and R. W. Heath Jr., "Spatially sparse precoding in millimeter wave MIMO systems," *IEEE Trans. Wireless Commun.*, vol. 13, no. 3, pp. 1499–1513, Mar. 2014.

[4] R. Méndez-Rial, C. Rusu, N. González-Prelcic, and R. W. Heath, "Dictionary-free hybrid precoders and combiners for mmwave MIMO systems," in *IEEE Int. Workshop Signal Process. Adv. Wireless Commun. (SPAWC)*, Jun. 2015, pp. 151–155.

[5] C. Rusu, R. M. Rial, N. González-Prelcic, and R. W. Heath Jr., "Low complexity hybrid sparse precoding and combining in millimeter wave MIMO systems," in *IEEE Int. Conf. Commun.*, Jun. 2015, pp. 1340–1345.

[6] A. Alkhateeb, G. Leus, and R. W. Heath, "Limited feedback hybrid precoding for multi-user millimeter wave systems," *IEEE Trans. Wireless Commun.*, vol. 14, no. 11, pp. 6481–6494, Nov. 2015.

[7] A. Alkhateeb and R. W. Heath, "Frequency selective hybrid precoding for limited feedback millimeter wave systems," *IEEE Trans. Commun.*, vol. 64, no. 5, pp. 1801–1818, May 2016.

[8] R. Peng and Y. Tian, "Wideband hybrid precoder design in MU-MIMO based on channel angular information," in *IEEE Int. Workshop Signal Process. Adv. Wireless Commun. (SPAWC)*, Jul. 2017, pp. 1–5.

[9] S. Park, A. Alkhateeb, and R. W. Heath, "Dynamic subarrays for hybrid precoding in wideband mmwave MIMO systems," *IEEE Trans. Wireless Commun.*, vol. 16, no. 5, pp. 2907–2920, May 2017.

[10] F. Sohrabi and W. Yu, "Hybrid analog and digital beamforming for mmWave OFDM large-scale antenna arrays," *IEEE J. Sel. Areas Commun.*, vol. 35, no. 7, pp. 1432–1443, Jul. 2017.

[11] J. P. González-Coma, N. González-Prelcic, L. Castedo, and R. W. Heath, "Frequency selective multiuser hybrid precoding for mmwave systems with imperfect channel knowledge," in *Proc. Asilomar Conf. Signals, Syst., Comput.*, Nov. 2016, pp. 291–295.

[12] J. P. González-Coma, J. Rodríguez-Fernández, N. González-Prelcic, L. Castedo, and R. W. Heath, "Channel estimation and hybrid precoding for frequency selective multiuser mmwave MIMO systems," *IEEE J. Sel. Topics Signal Process.*, vol. 12, no. 2, pp. 353–367, May 2018.

[13] J. Rodríguez-Fernández and N. González-Prelcic, "Low-complexity multiuser hybrid precoding and combining for frequency selective millimeter wave systems," *IEEE Int. Workshop Signal Process. Adv. Wireless Commun. (SPAWC)*, 2018.

[14] M. Majumder, H. Saxena, S. Srivastava, and A. K. Jagannatham, "Optimal bit allocation-based hybrid precoder-combiner design techniques for mmWave MIMO-OFDM systems," *IEEE Access*, vol. 9, pp. 54 109–54 125, Apr. 2021.

[15] X. Yu, J. Zhang, and K. B. Letaief, "A hardware-efficient analog network structure for hybrid precoding in millimeter wave systems," *IEEE J. Sel. Topics Signal Process.*, vol. 12, no. 2, pp. 282–297, May 2018.

[16] J. S. Herd and M. D. Conway, "The evolution to modern phased array architectures," *Proc. IEEE*, vol. 104, no. 3, pp. 519–529, Mar. 2016.

[17] W. Yu and T. Lan, "Transmitter optimization for the multi-antenna downlink with per-antenna power constraints," *IEEE Trans. Signal Process.*, vol. 55, no. 6, pp. 2646–2660, Jun. 2007.

[18] Z. Pi, "Optimal MIMO transmission with per-antenna power constraints," in *IEEE Global Commun. Conf. (GLOBECOM)*, Jun. 2012, pp. 2493–2498.

[19] C. K. Thomas and D. Slock, "Hybrid beamforming design in multi-cell MU-MIMO systems with per-RF or per-antenna power constraints," in *88th IEEE Veh. Technol. Conf. (VTC-Fall)*, Aug. 2018.

[20] K. B. Dsouza, K. N. R. S. V. Prasad, and V. K. Bhargava, "Hybrid precoding with partially connected structure for millimeter wave massive MIMO OFDM: A parallel framework and feasibility analysis," *IEEE Trans. Wireless Commun.*, vol. 17, no. 12, pp. 8108–8122, Dec. 2018.

[21] J. S. Herd and M. D. Conway, "The evolution to modern phased array architectures," *Proc. IEEE*, vol. 104, pp. 519–529, Mar. 2016.

[22] T. M. Pham, R. Farrell, J. Dooley, E. Dutkiewicz, D. N. Nguyen, and L.-N. Tran, "Efficient zero-forcing precoder design for weighted sumrate maximization with per-antenna power constraint," *IEEE Trans. Veh. Technol.*, vol. 67, no. 4, pp. 3640–3645, Apr. 2018.

[23] M. Medra and T. N. Davidson, "Low-complexity robust MISO downlink precoder design with per-antenna power constraints," *IEEE Trans. Signal Process.*, vol. 66, no. 2, pp. 515–527, Jan. 2018.

[24] R. López-Valcarce, N. González-Prelcic, C. Rusu, and R. W. Heath, "Hybrid precoders and combiners for mmwave MIMO systems with per-antenna power constraints," in *IEEE Global Commun. Conf. (GLOBE-COM)*, Dec. 2016, pp. 1–6.

[25] P. L. Cao, T. J. Oechtering, and M. Skoglund, "Precoding design for massive MIMO systems with sub-connected architecture and per-antenna power constraints," in *22nd Int. ITG Workshop on Smart Antennas (WSA)*, Mar. 2018, pp. 1–6.

[26] J. Rodríguez-Fernández, R. López-Valcarce, and N. González-Prelcic, "Frequency-selective hybrid precoding and combining for mmWave MIMO systems with per-antenna power constraints,," in *Proc. IEEE Int. Conf. Acoust. Speech Signal Process. (ICASSP)*, May 2019.

[27] 3GPP, "Study on channel model for frequencies from 0.5 to 100 GHz (release 14)," *Tech. Rep. 38.901 v14.1.1*, Jul. 2017.

[28] Z. Zhou, J. Fang, L. Yang, H. Li, Z. Chen, and R. S. Blum, "Low-rank tensor decomposition-aided channel estimation for millimeter wave MIMO-OFDM systems," *IEEE J. Sel. Areas Commun.*, vol. 35, no. 7, Jul. 2017.

[29] K. Venugopal, A. Alkhateeb, N. González-Prelcic, and R. W. Heath Jr., "Channel estimation for hybrid architecture based wideband millimeter wave systems," *IEEE J. Sel. Areas Commun.*, vol. 35, no. 9, Sep. 2017.

[30] E. Vlachos, G. C. Alexandropoulos, and J. Thompson, "Wideband MIMO channel estimation for hybrid beamforming millimeter wave systems via random spatial sampling," *IEEE J. Sel. Topics Signal Process.*, vol. 13, no. 5, Sep. 2019.

[31] A. Brighente, M. Cerutti, M. Nicoli, S. Tomasin, and U. Spagnolini, "Estimation of wideband dynamic mmWave and THz channels for 5G systems and beyond," *IEEE J. Sel. Areas Commun.*, vol. 38, no. 9, Sep. 2020.

[32] P. Schniter and A. Sayeed, "Channel estimation and precoder design for millimeter-wave communications: The sparse way," in *Proc. Asilomar Conf. Signals, Syst., Comput.*, Nov. 2014, pp. 273–277.

[33] J. Rodríguez-Fernández and N. González-Prelcic, "Channel estimation for frequency-selective mmwave MIMO systems with beam-squint," *IEEE Global Commun. Conf. (GLOBECOM)*, Dec. 2018.

[34] J. H. Brady and A. M. Sayeed, "Wideband communication with high-dimensional arrays: New results and transceiver architectures," in *2015 IEEE Int. Conf. Commun. Workshop (ICC Workshop)*, Jun. 2015, pp. 1042–1047.

[35] R. Méndez-Rial, C. Rusu, N. González-Prelcic, A. Alkhateeb, and R. W. Heath Jr., "Hybrid MIMO architectures for millimeter wave communications: Phase shifters or switches?" *IEEE Access*, vol. 4, pp. 247–267, 2016.

[36] V. Garg, I. Santamaria, D. Ramirez, and L. L. Scharf, "Subspace averaging and order determination for source enumeration," *IEEE Trans. Signal Process.*, vol. 67, no. 11, pp. 3028–3041, Jun. 2019.

[37] R. A. Horn and C. R. Johnson, *Matrix Analysis*, 2nd ed. Cambridge University Press, 2013.

[38] C. Eckart and G. Young, "The approximation of one matrix by another of lower rank," *Psychometrika*, vol. 1, pp. 211–218, 1936.

[39] G. H. Golub and C. F. van Loan, *Matrix Computations*, 3rd ed. Johns Hopkins University Press, 1996.

[40] S. Jaeckel, L. Raschkowski, K. Borner, and L. Thiele, "QuaDRiGa: A 3-D Multi-Cell Channel Model With Time Evolution for Enabling Virtual Field Trials," *IEEE Trans. Antennas Propag.*, vol. 62, no. 6, pp. 3242–3256, Jun. 2014.

[41] S. Jaeckel, L. Raschkowski, K. Borner, L. Thiele, F. Burkhardt, and E. Eberlein, "QuaDRiGa: Quasi Deterministic Ratio Channel Generator, User Manual and Documentation," *Fraunhofer Heinrich Hertz Institute, Tech. Rep. v2.0.0*, 2017.

[42] K. Haneda *et al.*, "5G 3GPP-like channel models for outdoor urban microcellular and macrocellular environments,," in *83rd IEEE Veh. Technol. Conf. (VTC-Spring)*, May 2016.

[43] H. S. Witsenhausen, "A determinant maximization problem ocurring in the theory of data communication," *SIAM J. Appl. Math.*, vol. 29, no. 3, pp. 515–522, Nov. 1975.